THESIS FOR THE DEGREE OF DOCTOR OF PHILOSOPHY

Molecular Solar Thermal Energy Storage System: Evaluation of Different Candidates

Characterization, Modification and Integration into Devices

ZHIHANG WANG

Department of Chemistry and Chemical Engineering

CHALMERS UNIVERSITY OF TECHNOLOGY

Gothenburg, Sweden 2019

Molecular Solar Thermal Energy Storage System:
Evaluation of Different Candidates
Characterization, Modification and Integration into Devices
ZHIHANG WANG
ISBN 978-91-7905-184-6

Doktorsavhandlingar vid Chalmers tekniska högskola
Ny serie nr 4651
ISSN 0346-718X

Department of Chemistry and Chemical Engineering
Chalmers University of Technology
SE-412 96 Gothenburg
Sweden
Telephone + 46 (0)31-772 1000

Cover:
Artistic molecular solar thermal energy storage driven castle, inspired by *Howl's moving castle*, designed by Mariza Mone.

Chalmers Reproservice
Gothenburg, Sweden 2019

Abstract

MOLECULAR SOLAR THERMAL ENERGY STORAGE SYSTEM: EVALUATION OF DIFFERENT CANDIDATES

Characterization, Modification and Integration into Devices

ZHIHANG WANG

Department of Chemistry and Chemical Engineering
Chalmers University of Technology

The development of solar energy can potentially meet the growing requirements for a global energy system beyond fossil fuels, however necessitates new scalable technologies for solar energy storage. One approach is the development of energy storage systems based on molecular photoswitches, so-called molecular solar thermal energy storage (MOST). By using organic photoswitchable compounds, the material can absorb sunlight thus photoisomerized to a metastable high energy photoisomer for ideally a long period of storage time, in such way, solar energy can be transformed to chemical bond strength of the molecule. When energy is needed, the converted molecule can be passed through a catalytic fixed bed reactor to release efficiently the stored energy in the form of heat, which could be used for, in this instance, domestic heating and low-temperature industrial heating purposes. Various candidates have been proposed for MOST applications, however a systematic evaluation and comparison of the proposed candidates is still scare. Here in this thesis, three candidates with difference photoswitching mechanisms including a norbornadiene derivative, an azobenzene derivative, and a dihydroazulene derivative have been characterized in detail for their availability of MOST purposes. Some modifications of tested norbornadiene has been tried as a further effort to improve the molecules' properties. Later, all three candidates have been integrated into either indoor or outdoor devices for real application evaluations. Moreover, for stored energy release part, suitable catalysts for each candidate has been discovered, more discussion about future catalyst perspective have been performed in the context. Results show in a clear way how far this technology can be industrialized and the direction of next generation of MOST candidates.

Keywords: Solar Energy; Energy conversion; Energy storage and release; Thermal dynamics; Molecular switches; Norbornadiene; Quadricyclane; Azobenzene; Dihydroazulene; Vinylheptafulvene; Catalyst

To my parents, a gift that I have prepared for over ten years.

送给我的父亲母亲，一个准备了十年的礼物。

Acknowledgements

The *Knut and Alice Wallenberg Foundation*, *Swedish Foundation for Strategic Research* and *Chalmers University of Technology* are gratefully acknowledged.

I would like to deeply thank my supervisor, my mentor, Professor Kasper Moth-Poulsen. Thank you for accepting me as your Ph.D. student, to open this awesome journey for me. Thanks for your patience, inspiration, positive energy, optimism and all the chances that you give me to improve myself. Also, thanks for sharing those treasurable life and work experiences with me, I feel extreme lucky and truly appreciate it. I would also like to thank my co-supervisor Associate professor Karl Börjesson, for all your advices and guidance. Thanks for pushing me to be a good scientist.

Special Thanks to Dr. Martyn Jevric, brilliant organic chemist, writer, painter, the "Beast", Gammel Dansk, second place CS player (I'm the best of cause), and the most important, my best mate forever. I couldn't forget all those times we spend in the lab, without you, my Ph.D. life wouldn't be complete. Remember you, me and Mads, we were camping in alligator gorge, both of you slept so quietly in the van, just like two babies. And thanks for taking care of me especially for preparing a blanket. Again, as I told both of you, there are no wild bears in Australia.

Special Thanks to Dr. Mads Mansø, I still remember that your favorite hobby is to learn nice Chinese words, like "I love to eat sponge tofu, I like vegetables" etc.

Special Thanks to Dr. Anne Ugleholdt Petersen, my Dansk older sister. I still remember that you, Martyn and me, we were singing Charismas songs in a Karaoke bar in China, with nice orange juice.

Special thanks to Mariza Mone, brilliant artist, a lovely Greek girl, also delicious Greek cake maker. Thanks for designing this awesome cover for me. You have no idea how much I love this cover.

Special thanks to Dr. Jessica Orrego Hernandez, for encouraging me to keep going, for your patience in teaching me organic chemistry. Thanks for sharing those touchable study stories

with me, and let me know the power of being positive. Also, don't forget to tell me the address of your coffee shop in Paris!

Special thanks to Dr. Sarah Lerch, for always helping me correct my English, at the same time being a good friend.

Thanks to Xin Wen, my officemate, for all the laughs and food that you bring to me. You are definitely a supportive friend! Thanks to Dr. Raul Losantos, my Spanish mate, hope we can work together again, I own you another beer. Thanks to Prof. Xiaofeng Xu, Prof. Liyang Yu, Dr. Zhaojun Li, Yidong Chen, Prof. Jiamin Cao, Prof. Nong Wang, Dr. Zhiyuan Cong, Dr. Qunping Fan, Dr. Wenyan Su, Dr. Amir Masoud Pourrahimi, Mengqiao Di, Yanyue Feng, Wenhong Peng, Alexei Cravcenco, Alicja Stolaś, Ulises Mendez Romero, Dr. Hakan Bildirir and Yifei Zhang. You guys make me feel home. Thanks to Maria Quant, Dr. Ambra Dreos, our awesome MOST team and all my colleagues on the 8th floor, for this wonderful working environment with laughs and fun. Thanks to Lotta Pettersson, our awesome administrator. You have made my life much easier with all administrative papers. Nu jag kan prata Svenska!

Zhaoping Rong, my lovely girlfriend, thanks for your encouragement from nearly 7100 km away. Thanks for always telling me, be who you want to be. Love you so much. 亲爱的荣，我可爱的女朋友，谢谢你横贯了将近七千一百公里的支持，也谢谢你告诉我去做自己想做的事。爱你，想念你的点点滴滴。

Mam and Dad, thanks for telling me don't be afraid and just keep going during those hard times. Thanks for all those moments where you were waiting in front of the phone and worried about me. Thanks for all the continuous supports, loves, laughs, tears for more than ten years that I've been studying in Europe. I love you all so much. I hope that I am your proud, forever. 爸妈，谢谢你们长久以来最无私的支持，谢谢你们为我付出的那些爱，那些欢笑，那些泪水，那些十年来日日夜夜的期盼和饱含深情的惦念。我爱你们，希望我是你们的骄傲，永远的骄傲。

In the end, I would like to give the final thanks to my grandfather, the enlightenment teacher who stably encouraged me to learn science, to do research from the very beginning of my studies. 在最后，我想特别致谢我的外公，那个曾经如此坚定地让我走上科研道路的人。

List of Publications

1. Zhihang Wang, Anna Roffey, Raul Losantos, Anders Lennartson, Martyn Jevric, Anne U. Petersen, Maria Quant, Ambra Dreos, Xin Wen, Diego Sampedro, Karl Börjesson and Kasper Moth-Poulsen., *Energy Environ. Sci.*, 2019, **12**, 187–193. **(Cover Profile)**

2. Martyn Jevric, Zhihang Wang, Anne U. Petersen, Mads Mansø, Christopher J. Sumby, Mogens Brøndsted Nielsen, and Kasper Moth-Poulsen, *Eur. J. Org. Chem.*, 2019, **13**, 2354–2361.

3. Zhihang Wang, Raul Losantos, Diego Sampedro, Masa-aki Morikawa, Karl Börjesson, Nobuo Kimizuka and Kasper Moth-Poulsen, *J. Mater. Chem. A*, 2019, **7**, 15042–15047.

4. Zhihang Wang, Jonas Udmark, Karl Börjesson, Rita Rodrigues, Anna Roffey, Maria Abrahamsson, Mogens Brøndsted Nielsen, and Kasper Moth-Poulsen., *ChemSusChem*, 2017, **10**, 3049–3055. **(Cover Profile)**

Contribution report

1. Performed almost all the work, including TGA measurement, quantum yield measurements, cycling test, characterization of potential catalyst candidates, catalyst physisorption, outdoor test, macroscopic heat release. Wrote the first version of the manuscript.

2. Participated in developing the idea of the project, synthesized parts of the compounds, precipitated in characterizing the materials, and contribute to writing the manuscript together with other authors.

3. Performed almost all the work, including quantum yield measurements, cycling tests, characterization of the catalyst functionality in the device. Wrote the first version of the manuscript.

4. Performed almost all of the characterization work, cycling test, device theoretical simulation, indoor and outdoor test. Wrote the first version of the manuscript.

Related papers are not included in the thesis.

- Ambra Dreos, Zhihang Wang, Jonas Udmark, Anna Ström, Paul Erhart, Karl Börjesson, Mogens Brøndsted Nielsen and Kasper Moth-Poulsen., *Adv. Energy Mater.*, 2018, 8, 1703401. **(Cover Profile)**

- Ambra Dreos, Zhihang Wang, Behabitu Ergette Tebikachew, Kasper Moth-Poulsen, and Joakim Andréasson., *J. Phys. Chem. Lett.*, 2018, 9, 6174–6178.

- Ambra Dreos, Karl Börjesson, Zhihang Wang, Anna Roffey, Zack Norwood, Duncan Kushnir and Kasper Moth-Poulsen., *Energy Environ. Sci.*, 2017, 10, 728–734. **(Cover Profile)**

- Mads Mansø, Anne Ugleholdt Petersen, Zhihang Wang, Paul Erhart, Mogens Brøndsted Nielsen and Kasper Moth-Poulsen., *Nat. Commun.*, 2018, 9:1945.

- Anne Kunz, Andreas H Heindl, Ambra Dreos, Zhihang Wang, Kasper Moth-Poulsen, Jonathan Becker and Hermann Andreas Wegner, *ChemPlusChem*, 2019, 84, 1145–1148.

- Martyn Jevric, Anne U. Petersen, Mads Mansø, Sandeep Kumar Singh, Zhihang Wang, Ambra Dreos, Christopher Sumby, Mogens Brøndsted Nielsen, Karl Börjesson, Paul Erhart, and Kasper Moth-Poulsen., *Chem. Eur. J.*, 2018, 24, 12767–12772. **(Cover Profile)**

- Anne Ugleholdt Petersen, Anna I. Hofmann, Méritxell Fillols, Mads Mansø, Martyn Jevric, Zhihang Wang, Christopher J. Sumby, Christian Müller and Kasper Moth-Poulsen., *Adv. Sci.*, 2019, 6, 1900367.

- Christian Schuschke, Chantal Hohner, Martyn Jevric, Anne Ugleholdt Petersen, Zhihang Wang, Matthias Schwarz, Miroslav Kettner, Fabian Waidhas, Lukas Fromm, Christopher Sumby, Andreas Görling, Olaf Brummel, Kasper Moth-Poulsen and Jörg Libuda., *Nat. Commun.*, 2019, 10: 2384.

List of Abbreviation

$[A(\lambda)]$	Actual concentration
$[A_0(\lambda)]$	Initial concentration
C_{isomer}	Specific heat capacity of isomer molecule
$C_{solvent}$	Heat capacity of solvent
$E_{AM\ 1.5}(\lambda)$	Photon energy under AM 1.5
E_a	Activation energy with Arrhenius equation
I_0	Intensity of the incident light
I_T	Transmitted intensity
M_w	Molecular weight
N_A	Avogadro number
$Tran_{filter}(\lambda)$	Transmittance of the bandpass filter
c_{cata}	Concentration of the catalyst
k_B	Boltzmann constant
$t_{1/2}$	Half-life
Φ_{iso}	Quantum yield
η_{MOST}	Energy storage efficiency
ρ_{isomer}	Volumetric mass density of isomer
$\rho_{solvent}$	Volumetric mass density of solvent
^{1}H NMR	Proton NMR spectrum
AM 1.5	Air mass 1.5 standard
AZO	Azobenzene
$CDCl_3$	Deuterated chloroform
CO_2	Carbon dioxide
CoPc	Cobalt (II) phthalocyanine
CoPc@C	Cobalt (II) phthalocyanine on activated carbon support
D-A	Donor-acceptor system
DHA	Dihydroazulene
DSC	Differential scanning calorimetry
$FvRu_2$	Fulvalene-tetracarbonyl-diruthenium
h	Plank constant

HOMO	Highest occupied molecular orbital
LED	Light emitted diode
LUMO	Lowest unoccupied molecular orbital
MOST	Molecular solar thermal energy storage system
NBD	Norbornadiene
NMR	Nuclear magnetic resonance
QC	Quadricyclane
$\mathrm{T}(\lambda, c)$	Wavelength and concentration-dependent transmittance
TGA	Thermogravimetric analysis
TOF	Turn over frequency
TON	Turn over number
UV	Ultraviolet
VHF	Vinylheptafulvene
Vis	Visible
$\Delta G^{\ddagger}$	Gibbs free energy
$\Delta H^{\ddagger}_{cat}$	Catalyzed activation enthalpy
$\Delta H_{storage}$	Energy storage enthalpy
$\Delta H^{\ddagger}_{therm}$	Thermal activation enthalpy
$\Delta S^{\ddagger}$	Entropy
$A(\lambda)$	Wavelength-dependent absorbance
I	Photon flux
R	Gas constant
T	Temperature
V	Reaction volume
c	Concentration
k	Reaction rate constant
l	Optical pathlength
α	Pre-factor of Arrhenius equation
$\beta(t)$	Fraction of photon absorbed
$\varepsilon(\lambda)$	Molar absorptivity

ν	Optical frequency
$\dot{n}_{\text{parent}}$	Flow speed of parent molecule
$\alpha_{\text{conversion}}$	Conversion ratio
S	Irradiated area

Table of Contents

Chapter 1

Introduction

With an increasing world population, the demand for energy is rising rapidly every year. According to statistics from the BP plc (formerly The British Petroleum Company plc and BP Amoco plc), in 2018, the global energy consumption increased by 2.9% compared to 2017, which was the largest yearly growth since 2010.[1] On the other hand, the United Nations projects that the global population is estimated to reach 8.5 billion by 2030 and further, it will exceed 9.1 billion by 2050.[2] This continuously increasing population and rapid economic growth consequently give rise to a cumulative demand on energy, resulting in predictions that the energy consumption will certainly be doubled within the next 40 years.[3]

Considering as one of the world's consumable carbon sources, fossil fuels, including oil, coal and natural gas, are still the main resources consumed today. Statistical data shows that, in 2018, CO_2 emissions from the consumption of these resources grew by 2.0%, producing, again, the fastest expansion for many years, with an increase in emissions of around 0.6 gigatonnes over the previous year.[1, 4] However, CO_2 emissions from the combustion of these fossil fuels are causing serious environmental issues. In fact, the massive emissions of CO_2 have resulted in a significant increase in the average temperature of the Earth over the last 200 years, a trend that still continues today.[5] Consequently, various abnormal changes in the climate are an indication that the world is facing a global warming issue.[6-15]

To discuss the countermeasures of this potential risk for the whole planet, in 2016, 195 countries gathered together in Paris for a multilateral agreement, in an attempt to reduce the human impact on climate change. The 'Paris agreement' was intended to curb the global temperature rise to below 2 degrees above pre-industrial levels, while, at the same time, pursuing efforts to limit the temperature increase to 1.5 °C above pre-industrial levels. [16]

One potential solution to achieve the stipulations laid out in the Paris agreement is the development of sustainable energy sources. It is important to mention that, even though the demand for all fuels increased in 2019, the growth of demand was particularly strong for renewable energy sources. Most notably, after the establishment of the Paris agreement, in the power generation sector, the use of renewable energy increased by 14% in 2018, indicating that the energy production sector focus shifted towards renewable energy technologies. [17]

Regarding green energy sources, the Sun can be considered as one of the most abundant energy resources available on Earth. As shown in figure 1.1, the world energy consumption in 2015 was estimated as 18.5 TWy y^{-1}, while the total solar power that reached the Earth during that same year was around 23000 TWy y^{-1}. This can be interpreted that, with only seven hours of total irradiation from the Sun, all energy needed for mankind for an entire year can be fully supplied. Thus, being able to harvest and store even a small portion of the solar energy can certainly fulfil, or at least relieve, the pressure of the growing world energy requirements. [18, 19]

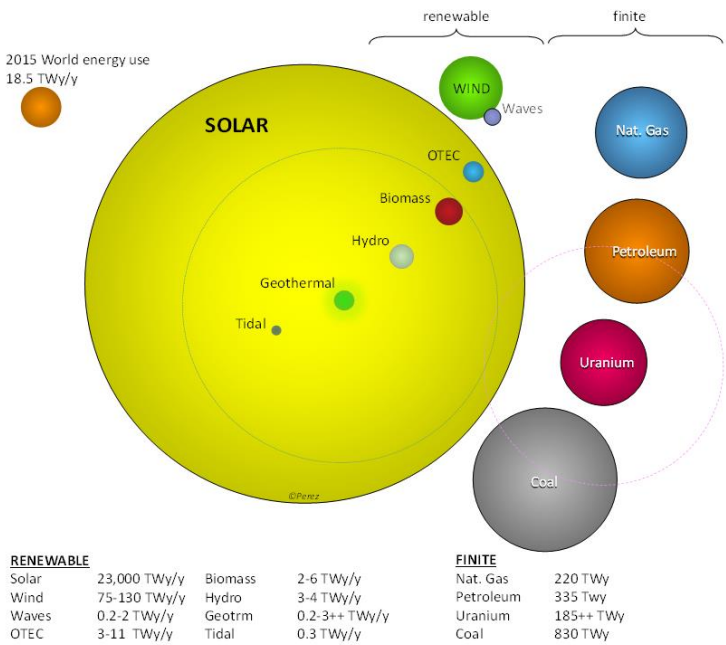

Figure 1.1: Estimated finite and renewable planetary energy reserves, for 2015 (Terawatt-years). Adapted from IEA SHC solar update 2015.

However, harvesting solar energy is quite challenging since efficient technologies to convert sunlight into secondary energy forms and a low loss energy grid are difficult to realize. Technically, it can be categorized into three parts: solar energy capture, conversion, and storage.[3] Some existing technologies already significantly impact the use and development of sustainable energy sources, such as photovoltaics,[20, 21] which capture and convert solar energy into electricity; artificial photosynthesis,[22-24] that captures, converts and stores solar energy for water-splitting; and solar thermal heating,[25, 26] which captures, converts and stores solar energy as heat.

The latest case, solar thermal technologies, refers to the transfer and storage sunlight to, sooner or later, be released in the form of heat. Heat consumption, such as low-temperature heat demand in industry and domestic heating, can be considered as the most important sector of energy consumption. In the European Union in 2017, household energy consumption resulted in 27.2% of the final energy consumption and thus, 17.2% of the gross inland energy consumption.[27] In addition, according to the statistical data of International energy agency (IEA), the average worldwide growth rate of solar thermal energy increased 11.2% from 1990 to 2017, demonstrating that solar thermal technology has gained increasing attention during recent decades.[17]

This thesis presents research efforts into a developing technology called molecular solar thermal energy storage (MOST,[28-30] also referred to as solar thermal fuels,[31] STF). Based on organic photoswitchable materials, such a system can ideally absorb sunlight, then store the sunlight for future use. When energy is required, the stored solar energy can be released efficiently, using a catalyst, and on-demand as heat, completely free of greenhouse emissions, and environmentally friendly. According to projections from the transparency market research, the unique characteristics of such a system will likely drive the solar thermal fuel market by 2027.[32]

The thesis starts with the introduction containing a fundamental background, and then, three photoswitchable candidates have been selected, characterized and discussed for MOST purposes. The presented work also includes detailed analysis in devices, thus building a more general view to guide future molecular design and system evaluations, and finally shows that MOST can potentially play a significant role in the future development of renewable solar energy, especially for periodic heating purposes such as night-time and

seasonal domestic heating and low-temperature heating purposes in housing and buildings.[29]

Chapter 2

Molecular Solar Thermal Energy Storage System (MOST)

In this chapter, the background and fundamental functioning mechanism of MOST is presented.

2.1 Photoswitchable molecules

In 1819, Grotthuß found a photobleaching process and stated that light can cause certain chemical reactions, but only if the irradiation light color matches to the absorption properties of the substance.[33] Further understanding of such photochemical processes did not progress much until the complete theory on how light interacts with the matter was described later in the nineteenth century. Nevertheless, there were more discoveries of photochromic species in the meantime.[34]

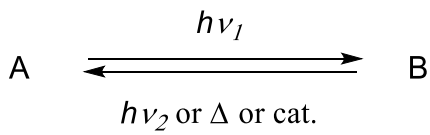

Scheme 2.1: Schematic illustration of photochromic molecules. A represents parent molecules, B corresponds to the high energy metastable photoisomer of A after irradiation. The back-conversion from B to A can be realized with light (different wavelength than the conversion process), heat or in the presence of a suitable catalyst.

Photoswitchable molecules, also called photochromism or photochromic compounds, are defined as compounds A (parent) that can undergo a photon-induced chemical reaction to isomer forms B (photoisomer), and later, switched back either by light (P-type), heat (T-type) or even catalyst-driven to the initial state A. (see Scheme 2.1)

Various types of photochromic materials in both inorganic and organic forms have been previously reported. For inorganic materials, this includes some metal oxides such as Hackmanite,[35] alkaline earth sulfides,[36] titanates, like silver loaded titanium dioxide thin film,[37] metal halides,[38] as well as some transition metal compounds, for instance, tungsten oxide[39] and molybdenum oxide.[40] The most well-known examples are silver halides which have been largely used in transition lenses.[41] Once exposed to sunlight, the transparent glasses will darken, because irradiating UV light can provide reduction reaction, thus forming darker elemental silver. While in shade, the material can be later oxidized to silver cations which are transparent. Inorganic photochromic compounds usually have good resistance to fatigue, i.e., they feature a large recycling charge and discharge number. However, the spectral difference between parent and photoisomer is not significant and, in addition, they often require a long response time.[42, 43]

Concerning organic photochromic compounds, the first organic photoswitchable chemical substance is considered to have been discovered by Fritzsche in 1867:[44] the reversible dimerization of anthracene molecules under irradiation, shown in scheme 2.2. It was found that the dimer can form crystals, which have a higher melting point than corresponding parent anthracene molecules. This reaction was then studied in detail later by Weigert.[45-48] He was, in fact, the first person to suggest that anthracene dimerization can be used for the purpose of solar energy storage and stated that at least 5% of the sunlight can be artificially converted into mechanical work. Therefore, his report could be considered as the first introduction to the MOST concept.

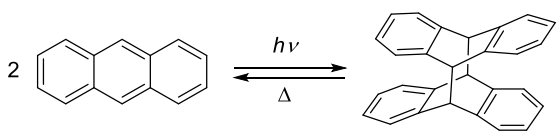

Scheme 2.2: Photon-induced dimerization of anthracene molecules, the first described organic photoswitchable material.

The applications for organic and organometallic photochromic materials are broad. They can be used for molecular machines,[49, 50] optical data storage,[51-55] single molecular electronics,[56-59] sensing,[60-64] liquid crystals[65-68] and bioimaging.[69] Several photoswitchable molecules are shown in scheme 2.3, below, including anthracene,[70-76] nitrones,[77-79] 3.5-diaryl-2-isoxazoline,[80] *endo*-tricyclo[5.2.1.02,6]deca-4,8-diene-3-one,[81] 1-ethoxycarbonyl-1H-azepine,[82] stilbene,[83, 84] dithienylethene,[85-89] azobenzene,[31, 49, 90-104] Dewar,[105] spiropyran,[106, 107] Stenhouse adducts,[108-110] norbornadiene,[28, 59, 93, 111-131] dihydroazulene,[57, 58, 119, 132-143] and fulvalene-tetracarbonyl-diruthenium.[29, 93, 144-148]

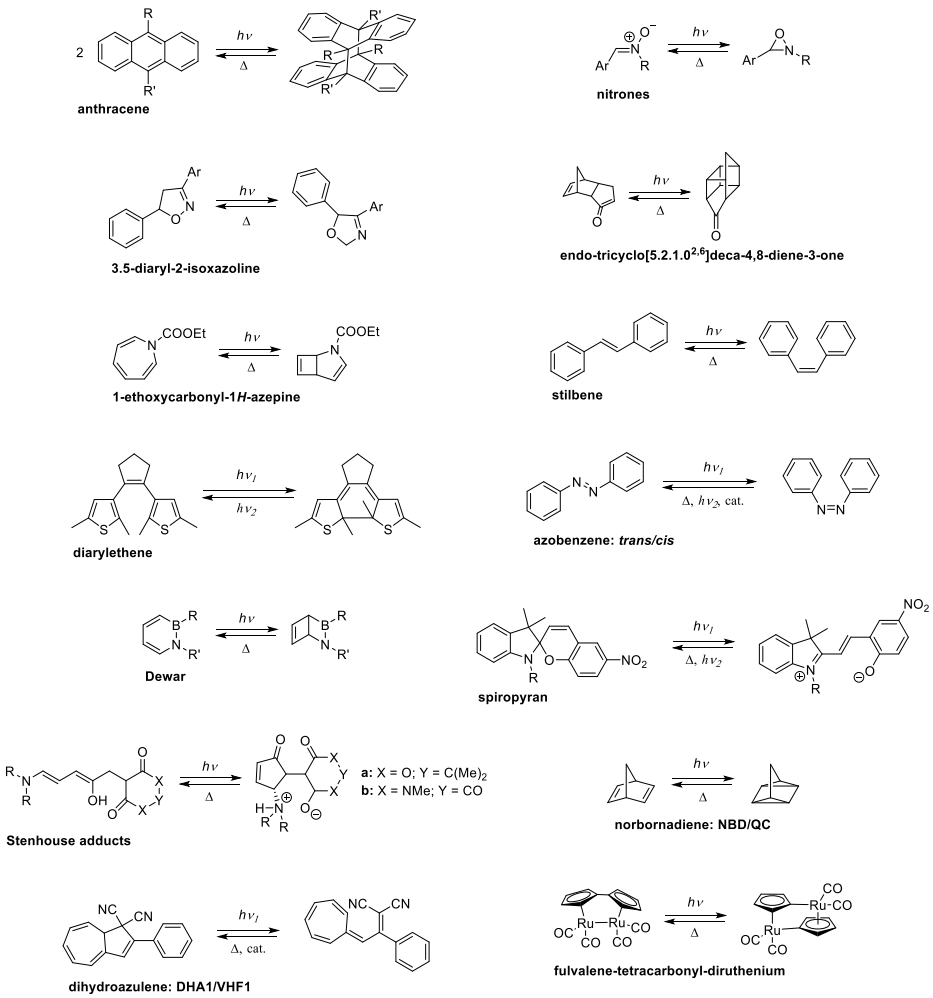

Scheme 2.3. Several reported photoswitchable couples, some of which have been pursued for solar energy storage applications.

Since the spectral properties of A and B are normally different, the molecules can be categorized as negative photochromism[149] or positive photochromism (see Figure 2.1).[150] The absorption profile of the parent state of the negative photochromic molecules is red-shifted compared to their absorption spectrum after irradiation with light, i.e. for the metastable. For instance, Chapter 4 features the negative photochromic molecule couple, an NBD/QC derivative (**NBD1**/**QC1**), which is represented in detail. The initial state of a positive photochromic molecule is normally blue-shifted compared to its corresponding photoisomer, and specific examples can be found in Chapter 5 for a DHA/VHF derivative (**DHA1**/**VHF1**) and an AZO *cis-trans* derivative (**AZO1**). In all these cases, some photochromic molecules are suggested and evaluated for solar energy storage purposes.

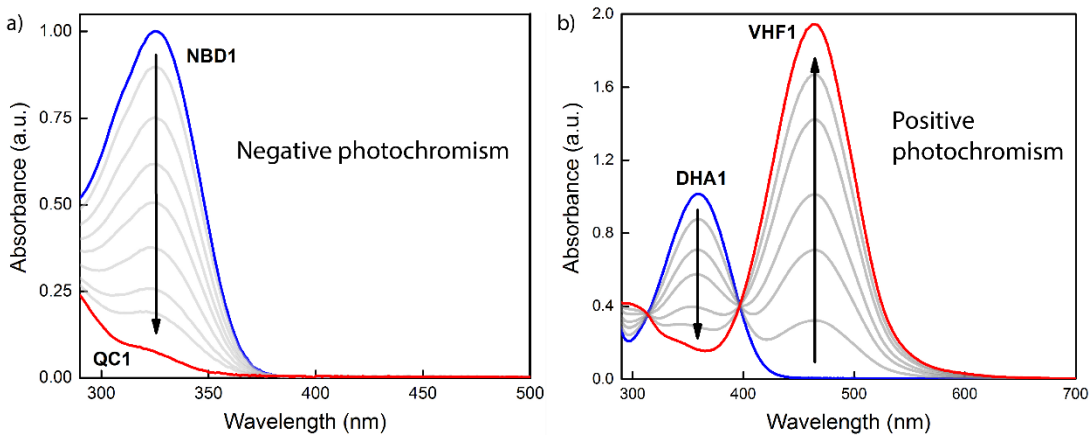

Figure 2.1. a) Progressive irradiation spectrum changes of a negative photochromic molecule couple, **NBD1/QC1**, as described in Chapter 4. b) Progressive irradiation spectrum changes of a positive photochromic molecule couple, **DHA1/VHF1**, as described in Chapter 5.

2.2 Photochromic compounds for molecular solar thermal energy storage purpose

Energy storage of photons in photoswitches requires the formation of new chemical bonds.[28, 29] As shown in figure 2.2a, the parent molecules (C) can absorb sunlight, be excited and photoisomerized to the high metastable energy state (D). The metastable D can then be stored, ideally over the years, for future use. When energy is required, with an efficient heat

source or a catalyst, the photoisomer can release the stored energy in form of latent heat "on-demand". The heat released from the reverse reaction can then be used for domestic heating purposes or even creating steam for secondary energy generation in the forms of electricity, mechanical energy, etc (see Figure 2.2b). This solar energy collection, materials charge/storage, and heat release process is called molecular solar thermal energy storage system (MOST).

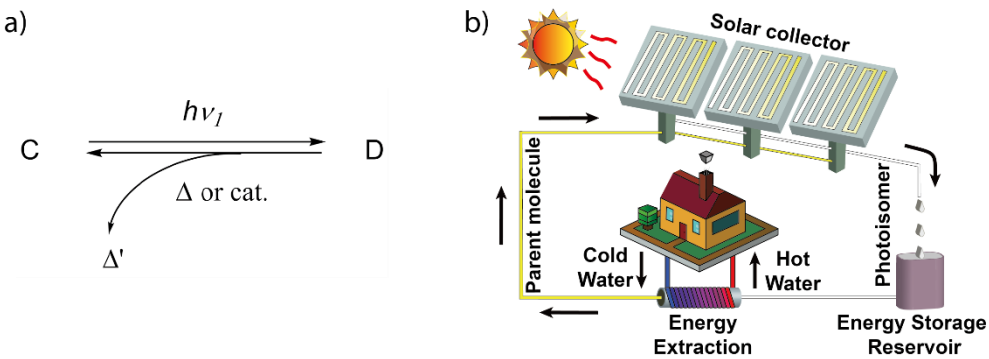

Figure 2.2. a) Schematic illustration of photoswitchable molecules for MOST application, where C represents the parent molecule. After absorbing sunlight, it can be charged to a high energetic photoisomer, D. The stored energy can be released either thermally or catalytically in the form of heat; b) Blueprint of a cycling MOST system from solar energy collection and storage to energy release for domestic heating. *© Reproduced with permission from the Royal Society of Chemistry.*

2.3 Basic criteria for MOST concept

In an energy diagram, the whole functioning process of MOST can be described as in figure 2.3. Various research studies show that modifications can eventually affect several properties, since all intrinsic properties of a given system are not completely independent from each other.[114, 128, 130] For instance, a low excitation energy of the system can potentially affect the back-conversion energy barrier, $\Delta H^{\ddagger}_{therm}$, at the same time, often reducing energy storage density, $\Delta H_{storage}$. [113]

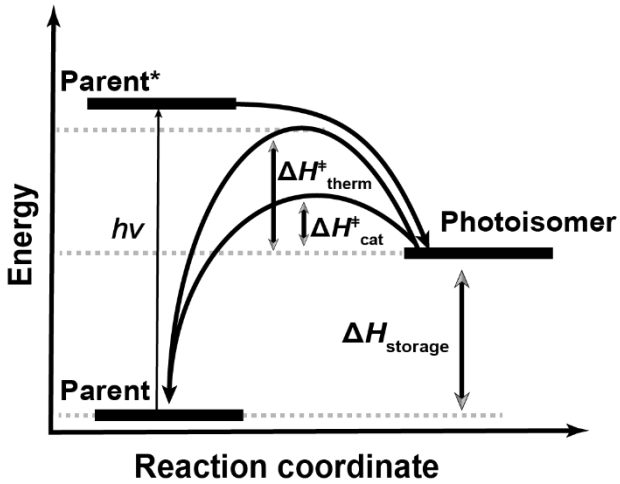

Figure 2.3. Energy diagram of the MOST system, where *hv* represents the energy to excite the molecule. $\Delta H^{\ddagger}_{therm}$ is the thermal activation energy of back conversion, $\Delta H^{\ddagger}_{cat}$ corresponds to the catalysis activation energy of back conversion. $\Delta H_{storage}$ is to the energy storage enthalpy. *© Reproduced with permission from the Royal Society of Chemistry.*

Therefore, some features are necessary for a good potential MOST system. All criteria have been well summarized and explained in earlier reports,[28, 111, 112, 147, 151] as:

1. The air mass (AM) 1.5 solar irradiation spectrum shows that more than 50% of the photons are between 300 nm to 800 nm. Therefore, the absorption spectrum of the parent molecules should be able to absorb in this broad spectral region.
2. The absorption wavelength of the photoisomer should preferably not overlap with the absorption wavelength of the parent molecules, and the photoisomer may not quench any sensitizer.
3. The photoisomerization quantum yield ϕ_{iso}, which describes the photoisomerization capacity of the photoisomer, is a unitless factor. In the ideal case, this factor should be as close to 100% as possible for an efficient conversion process.
4. Once charged, the high energy metastable photoisomer should have a long half-life $t_{1/2}$ at room temperature, in order to ensure an application-relevant storage period, which normally can consider to be daily, monthly, yearly or even longer storage periods.
5. As an energy storage media, the metastable photoisomer should have a high energy difference relative to the parent molecule. At the same time, the molecular weight should be as low as possible to maintain a high energy density of the MOST couple,

which literature suggests to be > 300 J g^{-1}, exceeding the heat stored in the salt hydrates ($\Delta H_{storage}$ = 250 J g^{-1}).

6. The charge and discharge repeating cycle should be able to withstand an infinite number of repetitions without any degradation of the photoswitchable compounds.
7. To easily collect charged compounds, store sunlight and release the energy, MOST materials should ideally be in liquid form or have a high solubility in an appropriate low specific heat capacity solvent. Additionally, MOST compounds can also include phase change properties for more advanced heat release purposes.
8. For liquid-based MOST applications, an appropriate heterogeneous catalyst should be employed for a rapid energy release of the charged photoisomer on demand.
9. For economical and sustainability purposes, MOST compounds should be easy and cheap to make on a large scale for industrial production and these materials should be environmentally benignant nontoxic.

With all the above criteria under consideration, ideal MOST candidates certainly need to be wisely designed. In previous literature, it was suggested that for an ideal MOST, which is able to absorb visible light, the molecular weight M_w should lie in the range around 130 g mol^{-1}.[128] At the same time, the activation energy, $\Delta H^{\ddagger}_{therm}$, which relates to the energy storage half-life, should be at least in the range of 110 kJ mol^{-1} for daily, 120 kJ mol^{-1} for seasonal or 140 kJ mol^{-1} for even longer energy storage periods at room temperature. Thus, assuming if the onset of absorption of an ideal parent molecule located at 656 nm or 685 nm, previous calculations estimated that the maximum energy conversion efficiency varies between 10.6% and 12.4%.[147]

2.4 Four photoswitchable couples in MOST research

Even though molecular photoswitches have been discovered over a long time, only a few photoswitchable couples have been investigated in detail for MOST purposes. Four photoswitchable pairs, including the *cis-trans* isomerization based AZO molecules, the reversible electronic [2+2π] cycloaddition reaction-based NBD couple, the 10π retrocyclization based **DHA1** couple and the noble organometallic photoreaction based fulvalene Ru complex ($FvRu_2$) have been proposed as candidate motifs for MOST (see

Scheme 2.4). A comparison of their intrinsic properties including absorption spectra, energy storage density, and molecular weights can be found in review from Sun et al. in 2019.[90] (see Table 2.1)

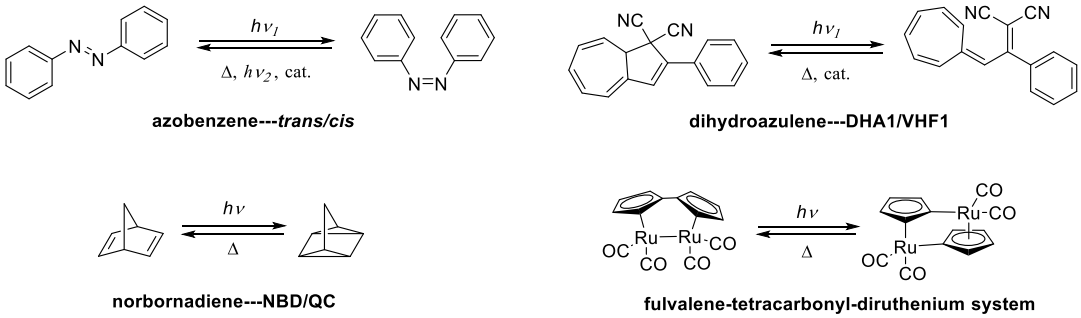

Scheme 2.4. Four photoswitchable molecules that have been proposed as MOST materials in literature.

Table 2.1. Key parameters of the four couples used in MOST research. See scheme 2.4 for molecular structures. MM stands for molar mass.

Photoswitch	$\lambda_{max,\ parent}$ (nm) [a]	Φ_{iso} (%)	$\lambda_{max,\ isomer}$ (nm) [a]	$\Delta H_{storage}$ (kJ mol^{-1})	$\Delta H^{\ddagger}_{therm}$ (kJ mol^{-1})	MM (g mol^{-1})
$FvRu_2$	~350	13%–17%	N/A	83±6	125±8	444
NBD/QC	213, 236	5%	<210	89±1	140	92
AZO *cis-trans*	~320	10%–35%	~450	49±5	95	182
DHA1/VHF1	~350	35%–55%	~470	~28	106	256

[a] *$\lambda_{max,\ parent}$: the maximum absorptive wavelength of parent isomer; $\lambda_{max,\ isomer}$: the maximum absorptive wavelength of the metastable isomer.*

Clearly, each photoswitch has its drawbacks as an ideal MOST system. The rare metal ruthenium-based material will not be suitable for industrialization. The absorption onset of unfunctionalized NBD/QC occurs in the UV region, poorly overlapping with the solar spectrum. Additionally, the photoisomerization quantum yield of NBD is too low to be applicable for further applications in devices. AZO and **DHA1** both posess relatively high molecular weights, thus, have lower energy storage density (MJ kg^{-1}) for energy storage purposes. Therefore, in the next chapters, with or without modification of the compounds, NBD/QC derivatives (**NBD1**/**QC1**), AZO *trans-cis* derivatives (**AZO1** *cis-trans*) and

DHA1/**VHF1** couples have been discussed for MOST availability and efforts for improvements of their intrinsic properties or working environments have been evaluated.

Chapter 3

Motivation and aims

As described in the previous chapter, an ideal photoswitchable couple still does not exist and as it should preferably address all the summarized criteria. Therefore, modifications based on different photochromic molecules to fit MOST purposes have been studied, with hundreds of different derivatives investigated in lab-scale experiments.[30, 90, 93] Yet, a systematic investigation, including solar capture, storage and stored energy release in applicable devices is currently scarce. Hence, the motivation of this thesis will mainly focus on a detailed evaluation of different MOST candidates consisting of several types of photoswitches in devices striving towards real application in the not too distant future.

To achieve this goal, NBD derivatives (**NBD1**) and two other MOST candidates (**AZO1**, **DHA1**) with different switchable mechanisms have been selected for detailed photophysical evaluations. Their unique properties reflect the intrinsic function of each compound, showing whether the materials are suitable for further MOST applications. Additionally, detailed characterizations will specify directions for future generations of the molecules. Since tested NBD derivative has overall an outstanding performance for MOST purpose, considering as a side project, some efforts to improve the existing properties of the tested NBD derivative have also been explored synthetically. From previous literature, extending the π-conjugation of donor-acceptor pair can potentially red shift the absorption spectrum towards a better overlap with the solar irradiation spectrum.[113] Therefore, the aim of such exploration focused on performing some small modifications to pre-existing compounds for supplementary amelioration. Subsequently, the three couples (**NBD1**, **AZO1** and **DHA1**) have been integrated into fluidic devices for real application tests, providing a functional overview of real life testing scenario.

As the last part of the MOST concept, catalyst design for a fast heat release is certainly necessary. To have an efficient on-demand energy collection, identification and applications of functional catalysts have also been studied and tested for each system. In the end, some detailed theoretical calculations for understanding the catalytic functioning mechanism have been proposed based on density functional theory, which is expected to inspire the future strategy of catalyst design.

With all the above experimental and theoretical efforts, it is possible to compare tested candidates systematically, while, at the same time, establishing a future evaluation protocol for all other MOST candidates, including preexisting and those made in future research. Such a protocol can hopefully increase the efficiency of testing a potential new MOST system. In this way, the gap between laboratory experiments and industrial production for real-life can be shortened, and consequently, implementation of MOST concept into real-life scenarios can be achieved in the near future.

Chapter 4

Methods

This chapter focuses on the theoretical background of the instruments and experimental methods used to evaluate the MOST system.

4.1 Jablonski diagram

The Jablonski diagram represents the electronic states of a molecule and possible transitions between those levels. It is the clearest way to describe the energy evolution of a certain molecule. A brief example of the energy levels and possible energy transfers between those levels is represented in figure 4.1.

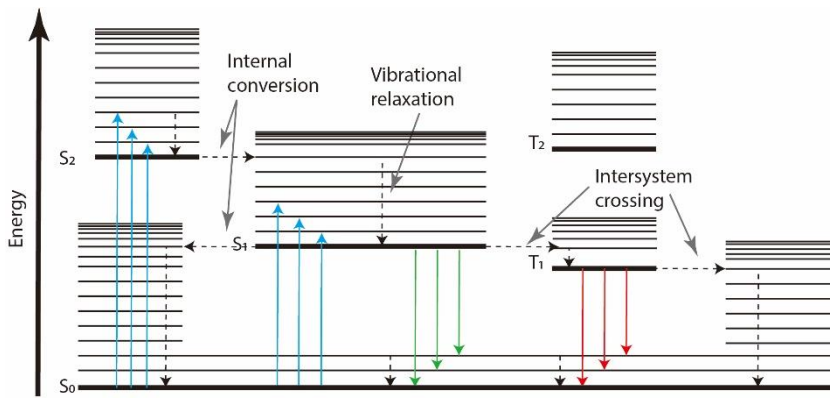

Figure 4.1. Jablonski diagram indicating different energy transfer processes between available energy levels: absorption (blue arrows), fluorescence (green arrows), phosphorescence (red arrows), internal conversion, intersystem crossing, and vibrational relaxation. Radiative and non-radiative transitions are represented by straight and dashed arrows, respectively. Energy states are indicated with horizontal black lines. Thick black lines correspond to electronic states, while the thin lines illustrate the different vibrational states present in each electronic state. S_n and T_n refer to the singlet and triplet states.

4.2 Absorption spectroscopy

To characterize the absorptivity, the thermal back-conversion half-life $t_{1/2}$ and to calculate the catalytic back-conversion rate, absorption spectroscopy is the most common and quantitative instrument to use.

The absorbance $A(\lambda)$ is determined with Equation 4-1, where I_0 is the intensity of the incident light and I_T is the transmitted intensity through the sample (see Figure 4.2):

$$A(\lambda) = \log(\frac{I_0}{I_T}) \tag{4-1}$$

At the same time, $A(\lambda)$ also depends on the concentration, c, of the prepared sample, the pathlength, l, of the light through the sample and the molar absorptivity, $\varepsilon(\lambda)$, of the molecule. This equation is known as the Beer-Lambert law[152]:

$$A(\lambda) = \varepsilon(\lambda) \cdot c \cdot l \tag{4-2}$$

With $\varepsilon(\lambda)$ in M^{-1} cm^{-1}, c in M and l in cm.

All experimental molar absorptivity values measured in this thesis are the mean value of absorptivity calculated from three individual measurements.

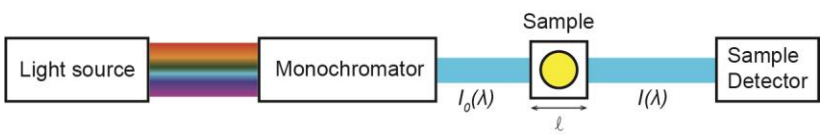

Figure 4.2: Schematic figure of a UV-Vis spectrophotometer.

4.3 Quantum yield for photoisomerization

The photoisomerization quantum yield, Φ_{iso}, for a reaction, as a unitless factor, is defined as the number of conversion reactions that have occurred divided by the number of photons absorbed.

For an ideal photoisomerization reaction, Φ_{iso} should be as close to unity (100%) as possible. Theoretically, for a photoswitchable molecule, the conversion and back-conversion process are shown in figure 4.3, where *a* and b correspond to the parent molecule and its converted photoisomer, respectively.

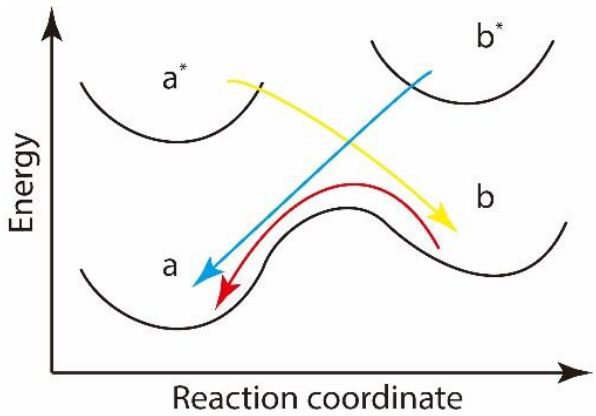

Figure 4.3: Energetic diagram of possible photochemical and thermal back-reaction processes. The yellow arrow shows the conversion process from a* (excited state of a) to b, while the blue arrow shows the photo-induced back-conversion process from excited photoisomer b* to ground state a. The red arrow shows the thermal back-conversion process from photoisomer b to a.

Therefore, for a solution of a single photoswitchable molecule, the concentration evolution due to irradiation can be expressed as:[153]

$$\frac{d[A(\lambda)](t)}{dt} = -\frac{\Phi_A I \beta_A(t)}{N_A V} + \frac{\Phi_B I \beta_B(t)}{N_A V} + k_{B\rightarrow A}[B(\lambda)] \qquad (4\text{-}3)$$

Where Φ_A, Φ_B represent the quantum yield of photon-induced conversion and back conversion, respectively; β_A, β_B refer to the fraction of photons absorbed by A, B, respectively; N_A is the Avogadro number; V is the reaction volume of the solution; $k_{B\rightarrow A}$ corresponds to the thermal back-conversion reaction rate constant in s^{-1}; and finally, I corresponds to the photon flux in Einstein s^{-1}, which can be determined using the ferrioxalate actinometer method, described below.

This method is based on the photochemical degradation of ferrioxalate, $Fe(C_2O_4)_3$ to Fe^{2+} in the presence of light. It was initially introduced by Parker and Hatchard.[154] The modified

detailed operating procedure can be found in a previously published article.[153] Thus, the ferrioxalate degradation reaction equations can be found as follows:

$$Fe(C_2O_4)_3^{3-} \xrightarrow{h\nu} Fe^{2+} + C_2O_4^{\cdot -} + 2C_2O_4^{2-} \tag{4-4}$$

$$Fe(C_2O_4)_3^{3-} + C_2O_4^{\cdot -} \xrightarrow{\Delta} Fe^{2+} + 2CO_2 + 3C_2O_4^{2-} \tag{4-5}$$

In this thesis, it has been assumed that the photon-induced back-conversion does not exist, and the thermal-induced back-conversion from state *b* to a can be ignored. Therefore, in equation 4-3, term $\beta_B(t)$ and the term $k_{B\to A}[B]$ are considered to equal zero. Experimentally, a solution with an absorbance above 2 at the irradiation wavelength is prepared, supposing that 99% of the light is absorbed by the solution. Thus, equation (4-3) can be simplified as:

$$[A(\lambda)](t) = [A_0(\lambda)] - \frac{\Phi_A I}{N_A V} t \tag{4-6}$$

Hence, by progressively irradiating the sample, the solution concentration and irradiation time, *t,* remain linearly dependent, and Φ_A can be fitted out.

For the Φ_{iso} measurements in this thesis, the experimental setup used consists of a UV-Vis spectrophotometer and a sample holder with four open access slots, a temperature controller and a magnetic stirring motor. In this setup, a sample can be irradiated with an appropriate collimated LED light source under a specific wavelength over a certain time period and then measured immediately with the UV-Vis spectrophotometer.

4.4 Kinetic studies for thermal back conversion

The thermal back-conversion of the photoisomer to the parent molecule can be described by a pseudo-first-order kinetic equation:

$$[A(\lambda)](t) = [A_0(\lambda)]e^{-kt} \tag{4-7}$$

Where $[A(\lambda)](t)$, $[A_0(\lambda)]$ are the actual and initial concentrations, respectively; k is the reaction rate constant in s^{-1} and t is the reaction time in s.

The half-life of the photoisomer at a specific temperature corresponds to a moment where $[A(\lambda)]$ equals $[A_0(\lambda)]/2$. From equation 4-7, it can be written as:

$$t_{1/2} = \frac{\ln(2)}{k} \tag{4-8}$$

This half-life actually depends on the thermal activation barrier of the back conversion. This energy barrier can be quantitatively described using either the Arrhenius equation or the Eyring equation.

As an empirical equation, the Arrhenius equation, which helps to qualify the reaction rate, is written as:

$$k = \alpha e^{-\frac{E_a}{RT}} \tag{4-9}$$

Where α represents a pre-exponential factor, a fingerprint constant for individual chemical reactions. According to collision theory, this factor refers to the collision frequency of the molecules with correct orientations. T refers to the temperature in k and R represents the gas constant in J K^{-1} mol^{-1}. Finally, E_a refers to the activation energy of the back-conversion in J mol^{-1}, which corresponds to the above-mentioned thermal activation energy barrier.

To account for the thermal dynamics, the energy description of a certain chemical reaction can be specified by the Gibbs free energy. Thus, the reaction rate constant k can, therefore, be described by the Eyring equation:

$$k = \frac{k_B T}{h} e^{-\frac{\Delta G^{\ddagger}}{RT}} \tag{4-10}$$

Where k_B is Boltzmann constant in J K^{-1}; h is the Plank constant in J s; $\Delta G^{\ddagger}$ refers to the Gibbs free energy in J mol^{-1}. In addition, the Gibbs energy can be written in relation to enthalpy and entropy:

$$\Delta G^{\ddagger} = \Delta H^{\ddagger}_{therm} - T\Delta S^{\ddagger} \quad (4\text{-}11)$$

Where $\Delta H^{\ddagger}_{therm}$ represents the activation enthalpy of the thermal back-conversion and $\Delta S^{\ddagger}$ is the entropy. Consequently, equation 4-10 can also be expressed as:

$$ln\frac{k}{T} = ln\frac{k_B}{h} - \frac{\Delta H^{\ddagger}{}_{therm}}{RT} + \frac{\Delta S^{\ddagger}}{R} \quad (4\text{-}12)$$

It can be seen that, at a specific temperature, $ln\frac{k}{T}$ is a linear equation dependent on $\frac{1}{T}$, and, therefore, experimentally $\Delta H^{\ddagger}_{therm}$, and $\Delta S^{\ddagger}$ can be fitted out.

To link E_a and $\Delta H^{\ddagger}_{therm}$, for a unimolecular, single-step reaction, a relation can be established:

$$E_a = \Delta H^{\ddagger}{}_{therm} + RT \quad (4\text{-}13)$$

However, due to the relatively small magnitude of $T\Delta S^{\ddagger}$ and RT, the values of E_a, $\Delta G^{\ddagger}$, and $\Delta H^{\ddagger}{}_{therm}$ are often conflated and all referred to as the "activation energy".

4.5 Cycling test

To test the cyclability of a given MOST candidate, a cycling test setup has been built with a UV-Vis spectrophotometer. A temperature tunable sample holder was installed inside the spectrometer.

For T-type back-conversion photoswitches, the temperature can be set high for a fast back-conversion. A time delay controllable LED source is programmed to convert the sample at defined time intervals.

Alternatively, for P-type back-conversion photoswitches, the sample holder temperature can be set at room temperature for the stabilization of the system. In this case, two-time

delay controllable LED sources are programmed to convert and back-convert the sample at defined time intervals. (see Figure 4.4)

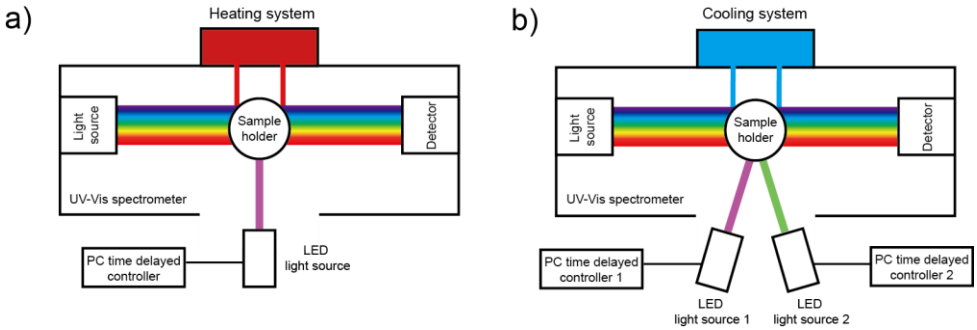

Figure 4.4: Experimental setup for the cycling test. a) T-type photoswitch cycling test setup, the LED light source is controlled by a time delay controller; b) P-type photoswitch cycling test setup, two LED light sources are controlled by two time delay controllers.

4.6 Differential scanning calorimetry and Thermogravimetric analysis

Differential scanning calorimetry (DSC) is a thermo-analytical technique that can measure the melting point and heat capacity of a material, as well as the energy release or consumption in e.g. phase change of molecular or polymer systems.

Instrumentally, two alumina pans are equally heated up simultaneously inside the DSC chamber; one of the pans contains the sample, and the other one is empty for a reference value. When the sample undergoes an endothermic heat absorption process, it will require more heat to increase the temperature compared to the reference. In the case of an exothermic heat release process, it will need less heat to balance the temperature compared to the reference. In this thesis, DSC is mainly used to measure the exothermic energy release process of the charged photoisomer state, resulting in a direct method to determine the energy storage capacity, $\Delta H_{storage}$.

Thermogravimetric analysis (TGA) can measure the maximum tolerance temperature of the chemical compound. When increasing the surrounding temperature, TGA measures the

mass change of the material. Indeed, it is important and necessary to know the thermal limit of MOST molecules in order to choose an optimum working temperature.

4.7 Catalytically driven back-conversion and heat release

To estimate the temperature which can be released from a charged photoisomer, a simplified equation, without taking into account the material phase, can be represented as:

$$\Delta T = \frac{c \cdot M_w \cdot \Delta H_{storage}}{c \cdot M_w \cdot C_{isomer} + \rho_{solvent} \cdot C_{solvent}} \quad (4\text{-}14)$$

Where c and M_w are the concentrations of the photoswitch and its corresponding molecular weight, respectively; C_{isomer} refers to the specific heat capacity of the material in J g^{-1} K^{-1}; $\rho_{solvent}$ and $C_{solvent}$ correspond to the volumetric mass density in g L^{-1} and the specific heat capacity in J g^{-1} K^{-1} of the solvent, respectively.

However, this estimation is not accurate for a liquid-phase material, since a neat compound will not involve any solvent dependency. Therefore, equation 4-14 should be rewritten as:

$$\Delta T = \frac{c \cdot M_w \cdot \Delta H_{storage}}{\frac{c^2 \cdot M_w^2}{\rho_{isomer}} \cdot C_{isomer} + (1 - \frac{c \cdot M_w}{\rho_{isomer}})\rho_{solvent} \cdot C_{solvent}} \quad (4\text{-}15)$$

With this approach, the volume load factor of the solvent $(1 - \frac{c \cdot M_w}{\rho_{isomer}})$, and photoisomer $\frac{c \cdot M_w}{\rho_{isomer}}$, were considered, i.e. when the concentration approaches neat conditions, the $(1 - \frac{c \cdot M_w}{\rho_{AZO1}})\rho_{solvent} \cdot C_{p\_solvent}$ approaches to zero. Compared to the first approximation, this correction is reasonable for all MOST candidates with close to neat conditions.

4.8 Conversion percentage determination with isosbestic point

To calculate the conversion percentage for a solution where a mixture of parent and photoisomer molecules co-exist in the solution, a determination method with isosbestic points can be used. For instance, figure 4.5 represents a spectrum of the **AZO1** solution where the conversion process is ongoing.

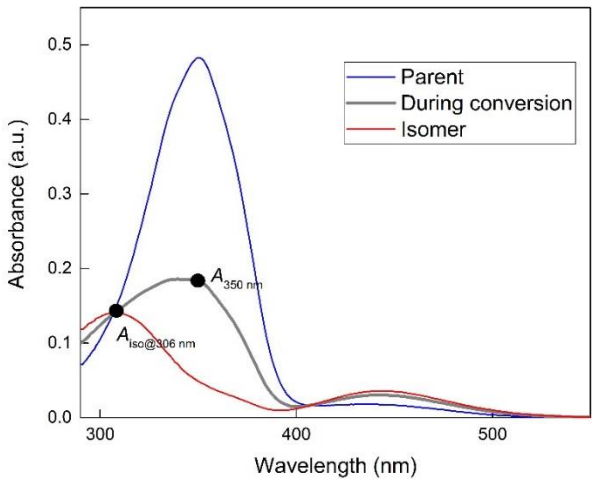

Figure 4.5. Spectral changes over the photoconversion process. The blue curve shows the pure parent state, the red curve shows the converted photoisomer form. Grey curve represents a spectrum taken during conversion. $A_{350\ nm}$ is the absorbance at 350 nm during conversion. $A_{iso@306nm}$ corresponds to the absorbance at the isosbestic point at 306 nm.

The absorbance at the isosbestic point can be expressed as:

$$A_{iso@306\ nm} = c_{parent}\varepsilon_{iso@306\ nm}l + c_{isomer}\varepsilon_{iso@306\ nm}l \tag{4-16}$$

Where c_{parent} is the concentration of parent state solution; $\varepsilon_{iso@306\ nm}$ is isosbestic absorptivity at 306 nm; c_{isomer} represents the concentration of photoisomer state solution.

This can be re-written as:

$$c_{parent} = \frac{A_{iso@306\ nm}}{\varepsilon_{iso@306\ nm}l} - c_{isomer} \tag{4-17}$$

Meanwhile, at 350 nm:

$$\varepsilon_{parent@350\ nm} c_{parent} l + \varepsilon_{isomer@350\ nm} c_{isomer} l = A_{@350nm} \tag{4-18}$$

Therefore, replacing c_{parent} with (4-17):

$$c_{isomer} = \frac{A_{@350\ nm}\varepsilon_{iso} - A_{iso@306\ nm}\varepsilon_{isomer@350\ nm}}{(\varepsilon_{parent@350\ nm} - \varepsilon_{isomer@350\ nm})\varepsilon_{iso@306\ nm} l} \tag{4-19}$$

It is known that the concentration of the prepared solution can also be calculated using the absorptivity at the isosbestic point:

$$c_{tot} = \frac{A_{iso@306\ nm}}{\varepsilon_{iso@306\ nm} l} \tag{4-20}$$

Therefore, it leads to a formula for the conversion percentage written as:

$$\text{Conversion } \% = \frac{c_{isomer}}{c_{tot}} \cdot 100\% = \frac{\frac{A_{@350\ nm}}{A_{iso@306\ nm}} \cdot \varepsilon_{iso@306\ nm} - \varepsilon_{isomer@350nm}}{\varepsilon_{parent@350\ nm} - \varepsilon_{isomer@350\ nm}} \tag{4-21}$$

Which can be used to calculate the conversion percentage during the conversion process.

4.9 Energy storage efficiency

The maximum energy storage efficiency can be calculated with equation 4-22:

$$\eta_{MOST} = \frac{\int_0^{\lambda_{onset}} \frac{E_{AM\ 1.5}(\lambda) \cdot (1 - \mathrm{T}(\lambda, c)) \cdot \phi_{iso} \cdot \Delta H_{storage}}{h\nu \cdot N_A} \cdot d\lambda}{\int E_{AM\ 1.5}(\lambda) \cdot d\lambda} \cdot 100\ \% \tag{4-22}$$

For certain photoswitches, optical bandpass filter can be used, therefore, the maximum energy storage efficiency can be calculated with bandpass filter by equation 4-23:

$$\eta_{MOST} = \frac{\int_0^{\lambda_{onset}} \frac{E_{AM\ 1.5}(\lambda) \cdot Tran_{filter}(\lambda) \cdot (1 - \mathrm{T}(\lambda, c)) \cdot \phi_{iso} \cdot \Delta H_{storage}}{h\nu \cdot N_A} \cdot d\lambda}{\int E_{AM\ 1.5}(\lambda) \cdot Tran_{filter}(\lambda) \cdot d\lambda} \cdot 100\ \% \quad (4\text{-}23)$$

Where $\mathrm{T}(\lambda, c)$ is the wavelength and concentration-dependent transmittance in a specific device with a specific optical pathlength. And $Tran_{filter}(\lambda)$ is the transmittance of the bandpass filter, this term equals 1 when no bandpass filter is used.

For a fluidic conversion experiment, the experimental energy storage efficiency with different residence time in a certain device can be calculated as:

$$\eta_{\mathrm{MOST}} = \frac{\dot{n}_{\mathrm{parent}} \cdot \alpha_{\mathrm{conversion}} \cdot \Delta H_{\mathrm{storage}}}{S \cdot \int E_{\mathrm{AM\ 1.5}}(\lambda) \cdot d\lambda} \quad (4\text{-}24)$$

Where $\dot{n}_{\mathrm{parent}}$ is the flow speed of parent molecule in mol s^{-1}, $\alpha_{\mathrm{conversion}}$ is the conversion ratio from parent state to photoisomer and S is the irradiated area in m^2.

4.10 Catalysis rate constant, turn over number and turn over frequency

To qualitatively and quantitatively check the functionality of a catalyst candidate, ^{1}H NMR experiments, the catalysis rate constant, turn over number and frequency are necessary to achieve.

Conversion determination using ^{1}H NMR

To check the activity of a potential catalyst, the switchable compound was initially dissolved in $CDCl_3$ or toluene-d_8 and a ^{1}H NMR spectrum was taken to check the purity of the sample. The sample is then irradiated using a lamp at an appropriate wavelength until a full conversion was obtained, where a second ^{1}H NMR spectrum was obtained. Next, the potential catalyst was added to the NMR tube containing the metastable compounds, incubated for a short period (typically much shorter than the half-life of the photoisomer), then checked using ^{1}H NMR again to determine whether a catalytic back-conversion has occurred.

Catalysis rate constant determined by UV-Vis

The catalysis triggered back-conversion curve can be fitted by the pseudo-first-order kinetic model:

$$y(t) = y_0 + A_1 e^{-k\, c_{cata}\,(t-t_0)} \tag{4-25}$$

Where k is the reaction constant; c_{cata} represents the concentration of the catalyst, assuming the suspension of the insoluble catalyst was homogeneously distributed in the solution; t represents the variable of time in s and y_0, A_1 are unitless parameters from the fit.

Turn over number (TON) and turn over frequency (TOF)

The performance of the catalyst can be described by the Turn over number (TON) and Turn over frequency (TOF).

The TON is defined as the maximum number of chemical reactions occurring in a single catalyst site before depletion:

$$\mathrm{TON} = \frac{\text{mol of the product (mol)}}{\text{mol of the reacted catalyst (mol)}} \tag{4-26}$$

In order to quantify this factor on a time scale, the Turn over frequency (TOF) is introduced. It can be calculated by using TON divided by the functional time of the catalyst before depletion, supposing a full catalytic conversion has been achieved:

$$\mathrm{TOF}\ (\mathrm{s}^{-1}) = \frac{\mathrm{TON}}{\text{functional time of the catalyst (s)}} \tag{4-27}$$

4.11 Photoswitching mechanisms and synthesis methods

In this thesis, few chemical reactions have been involved. This section briefly lists some key reactions.

Pericyclic reaction and Woodward-Hoffmann rules

AZO based photoswitching molecules follow *cis-trans* isomerization mechanism, NBD and DHA based compounds follow pericyclic photoswitching mechanism.

A pericyclic reaction is a rearrangement of π-electrons in a conjugated system, wherein the transition state of the molecules contains cyclic geometry. Woodward-Hoffmann rules can be used as a set of criteria to predict whether a pericyclic mechanism for a reaction is favorable. Typically, depends on the number of π-electrons involved in the reaction, the reaction condition can be different either by heat or light, thus hint the rotation direction of the bonds, providing a specific stereochemistry of the cyclic product (conrotatory and disrotatory, see Table 4.1 and Scheme 4.1). At the same time, the orbital symmetry conservation before and after the reaction need to be fulfilled in most of the cases. Therefore, those rules can predict most of the reaction conditions.

Table 4.1. The relation between the number of π-electrons, the trigger of reaction, and the reaction mode.

No. of π-electrons	Trigger of reaction	Reaction mode
4n	Δ	Conrotatory
	hv	Disrotatory
4n+2	Δ	Disrotatory
	hv	Conrotatory

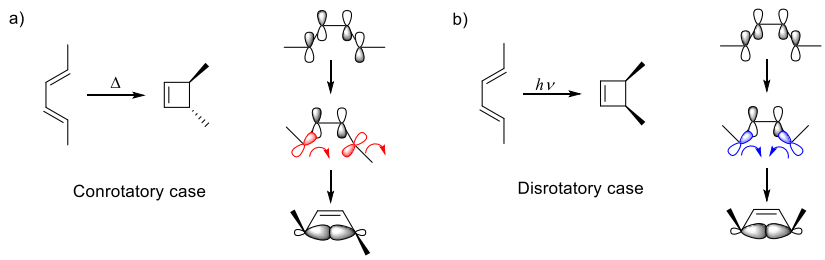

Scheme 4.1. Example of the stereospecifity of the electrocyclic ring-closure (conrotatory and disrotatory) of the substituted buta-1,3-diene, by a) heat condition and by b) light condition.

The Horner-Wadsworth-Emmons olefination and the Wittig reaction

Aldehyde moiety is a versatile functional group for extension of the π-system. A reaction such as Horner-Wadsworth-Emmons or Wittig with a stabilized phosphonate (Horner-

Wadsworth-Emmons)[155] or phosphonium salt (Wittig)[156] is convenient for achieving this extension while at the same time maintaining other units in the structure.

The Horner-Wadsworth-Emmons reaction starts with deprotonation of the phosphonate starting material, producing nucleophilic carbanion containing intermediate (**a**). Afterward, (**a**) will add onto the aldehyde group (**b**) through the nucleophilic addition reaction resulting **3a** or **3b**. The intermediates **3a** and **4a**, **3b** and **4b** can interconvert with each other. Finally, **4a** and **4b** (oxaphosphetane) will yield *E*-state of **c** and *Z* state of **d** by a reaction eliminating an organophosphate, with by-product of dialkyl-phosphate. This reaction typically favors the *E*-isomer. (*trans*, See Scheme 4.2)

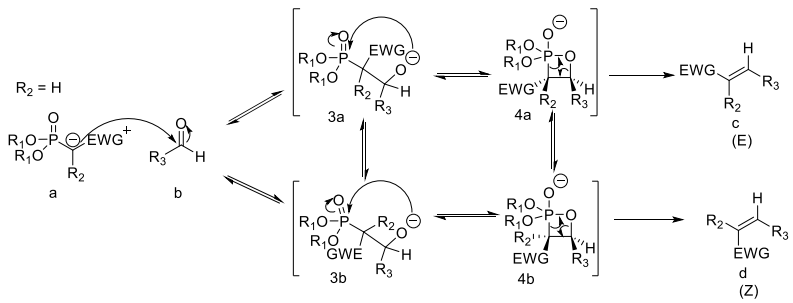

Scheme 4.2. The Horner-Wadsworth-Emmons reaction mechanism.

For Wittig reaction, a stabilized ylide (**a**) can react with the aldehyde group (**b**) through the nucleophilic addition reaction resulting in **3a** or **3b**. As intermediate products, **3a** and **4a**, **3b** and **4b** can interconvert with each other. Finally, **4a** and **4b** (oxaphosphetane) will yield *E*-state of **c** and *Z* state of **d** by rearrangement reaction, with a by-product of phosphine oxide, this reaction also favors *E*-state. (*trans*, See Scheme 4.3)

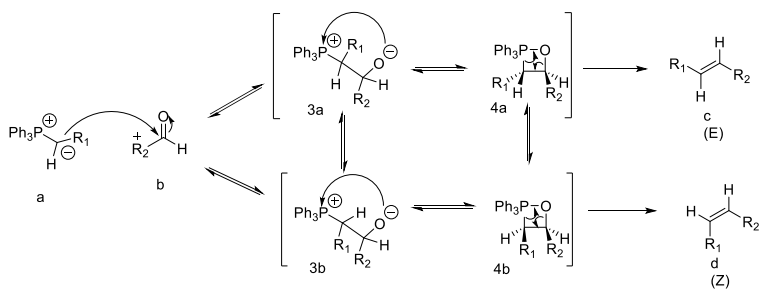

Scheme 4.3. The Wittig reaction mechanism.

Chapter 5

Norbornadiene/Quadricyclane based photoswitches for MOST

In this chapter, an NBD derivative with outstanding MOST performance has been characterized in detail, further integrated into devices for both energy storage tests and heat release experiments. This NBD derivative has also been chemically modified to observe its enhanced performance for MOST behavior. (Paper I, II)

5.1 Introduction

In the year of 1931, norbornadiene-2,3-dicarboxylic acid, and a dimethyl ester derivative were synthesized by Diels-Alder reactions starting from cyclopentadiene and acetylene dicarboxylic acid or acetylene dicarboxylic acid dimethyl ester, respectively.[157] It took until 1951, for unsubstituted norbornadiene to be first synthesized.[158] This unsubstituted material, providing a 3-dimensional geometry, also named bicyclo[2.2.1]hepta-2,5-diene, which contains two unconjugated double bonds, is a bicyclic organic compound. Such molecular geometry of the two double bonds is in close proximity enables possible intramolecular [2+2π] cyclization reactions. Thus, several efforts to prepare norbornadiene's (NBD) strained isomer form, quadricyclane (QC), via a synthetic route was made, however all failed. Later, Cristol and Snell's found that, a diacid derivative, under UV irradiation, can undergo a [2+2π] cycloaddition reaction forming QC diacid derivatives.[159] Therefore, in 1961, the first photoisomerization of parent NBD to QC was observed by direct

irradiation with UV light,[160] and also, it was independently demonstrated to work in the presence of a triplet sensitizer.[161]

With quite special properties, NBD, as the thermally stable parent molecule, can only convert to the corresponding QC through light irradiation. QC was found to be thermally (T-type) active in back converting to NBD. This conversion and T-type reverse reaction can be explained by Woodward-Hoffmann rules. [162-164]

It is noteworthy to mention that the energy level of NBD is about 145 kJ mol^{-1},[165] while the strain energy of QC can reach as high as 402 kJ mol^{-1},[166] more than two times higher than the energy of NBD. Of that strained energy, 92 kJ mol^{-1} can experimentally be released as heat, enough to vaporize water since that enthalpy only equals to 40.7 kJ mol^{-1}. Meanwhile, QC has a relatively long half-life of 655 hours in benzene under air at 293 K,[167] providing an extremely long storage time at ambient temperature. Nowadays, NBD is commercially available at reasonable prices (31.5 USD for 5 mL, Sigma Aldrich, 2019) from chemical companies. As mentioned in the previous chapter, an ideal MOST is preferably in liquid form. Both NBD and QC are liquid, and thus, easy to pump through a solar collecting device, and store in a chemical reservoir for later use.

Based on energetic criteria, NBD seems a good energy storage medium to harvest sunlight into chemical energy for future use. Yet, even though unsubstituted NBD can be one fascinating candidate, some drawbacks still remain. For instance, its absorption spectrum barely covers any solar spectrum, as it only absorbs in the UV, thus cannot be used directly for solar energy conversion and storage purposes. Conversion of NBD molecules need to be accompanied by a photosensitizer such as benzophenone or acetophenone. In addition, the photoisomerization quantum yield ϕ_{iso} determined for this process is only 9%. Therefore for practical use, it is necessary to chemically modify the NBD core by connecting different π-conjugated substituents to one or both olefins.

In the 1980s and 1990s, a large number of substituted NBDs were designed and synthesized mainly by two groups: Yoshida et al. in Japan and Dubonosov et al. in Russia.[28, 111, 112] Yoshida introduced, in 1985, a new concept of “donor-acceptor” (D-A) to redshift the absorption of norbornadiene (Figure 5.1 a). This gives a greater degree of red shifting for relative molecular weight added to the molecule, so as to keep the energy density as high as possible.

As shown in scheme 5.1b (1), the interaction of electron-donating groups at one side of the olefin double bond with electron-accepting groups through space, forming a homocoupling can result in a long-wave absorption edge as high as 500 – 560 nm. However, the molecular mass of those molecules is relatively high resulting in a low energy density.

The synthesis of type (1) norbornadiene derivatives faces a lot of difficulties: polysubstituted cyclopentadiene derivatives and disubstituted acetylene need to be firstly synthesized, then brought into Diels-Alder reaction. Later on, studies have shown that, in many cases, a pair of a single electron-donating group and a single electron-accepting group on one side of the olefin (2 in Scheme 5.1b) is enough to redshift the spectrum, thus giving similar or even better spectral qualities than D-A on both sides.[151] Therefore, the substitution of NBD in such a way has been selected as the main direction for current MOST candidates.

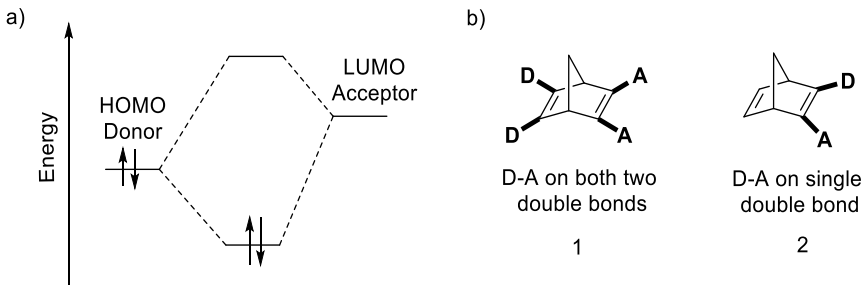

Scheme 5.1. a) Energy correlation diagram of a donor-acceptor based system; b) Two NBD donor-acceptor (D-A) molecular forms, with D-A on a single double bond (1), D-A on both double bonds (2).

5.2 Characterization of a new push-pull NBD1 molecule

The synthesis of type (2) norbornadiene derivatives (Scheme 5.1) can be done by either a simple Diels-Alder reaction between cyclopentadiene and a sufficiently activated acetylene or via coupling reactions to pre-existing NBD derivatives. Base on this strategy, a new donor (phenol methoxy group)-acceptor (cyano group) based **NBD1** has been synthesized. (**NBD1** in Scheme 4.1). In this instance, two synthetic pathways have been developed for producing **NBD1**, including a Suzuki coupling reaction with a palladium catalyst (**Method 1** in Scheme 5.2), or a direct Diels-Alder reaction from the cyclopentadiene and the 3-(4-

methoxyphenyl)propionitrile in the microwave (**Method 2** in Scheme 5.2). The author of this thesis did not participate in the synthesis work, and therefore, only the reaction steps are shown, without presenting detailed synthesis notes. It should be noted that for the latter method, **NBD1** can be easily synthesized both avoiding the use of inorganic toxic cyanide and costly catalyst reagents, at the same time on a large scale (ca. 10 g).

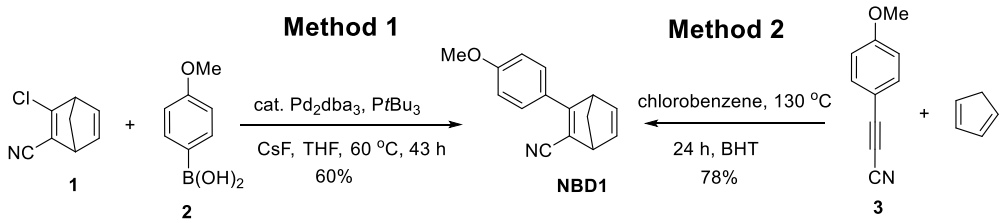

Scheme 5.2. Two methods for the synthesis of **NBD1**. **Method 1** uses a Suzuki coupling reaction as the key step; **Method 2** instead uses a Diels-Alder reaction approach.

To assess the photophysical properties of **NBD1** (see Figure 5.1a), toluene was selected as the solvent because of its non-polarity properties, and low specific heat capacity for later heat release purposes. A comprehensive characterization including a comparison of absorption spectra between **NBD1** and corresponding metastable **QC1**, the photoisomerization quantum yield, the thermal back-conversion half-life, and the cyclability studies. These data are presented in Figure 5.1. From the results, it can be seen that the absorption onset blue-shifts upon progressive irradiation. The maximum molar absorptivity for **NBD1** is ε_{max} = 1.3 x 10^4 M^{-1} cm^{-1} at λ_{max} = 326 nm, with the onset of absorption beginning at 380 nm (defined as the wavelength of an absorbance ≥ 100), thus providing a 4% absorption efficiency of the incoming photons from the solar spectrum. At the same time, the absorption spectrum of **QC1** is greatly diminished leaving a spectral window of 34 nm to fully convert **NBD1**. (see Figure 5.1b)

The ϕ_{iso} was measured as 61%, indicating that **QC1** can be easily formed via the photoisomerization reaction (Chapter 4, section 4.3). The half-life was performed with kinetic measurements using both Arrhenius and Eyring plot (Chapter 4, section 4.4), resulting in a $t_{1/2}$ of 30 days in toluene at room temperature.

Concerning the energy storage density, Differential scanning calorimetry (DSC) was used showing that the actual measured energy storage density equals 89 kJ mol^{-1}, thus corresponds to 0.4 MJ kg^{-1}, less than the value of the unsubstituted NBD. At the same time, this value is close to a typical Li-ion battery energy storage scale,[168] showing great potential for energy storage purpose. (see Figure 5.1c)

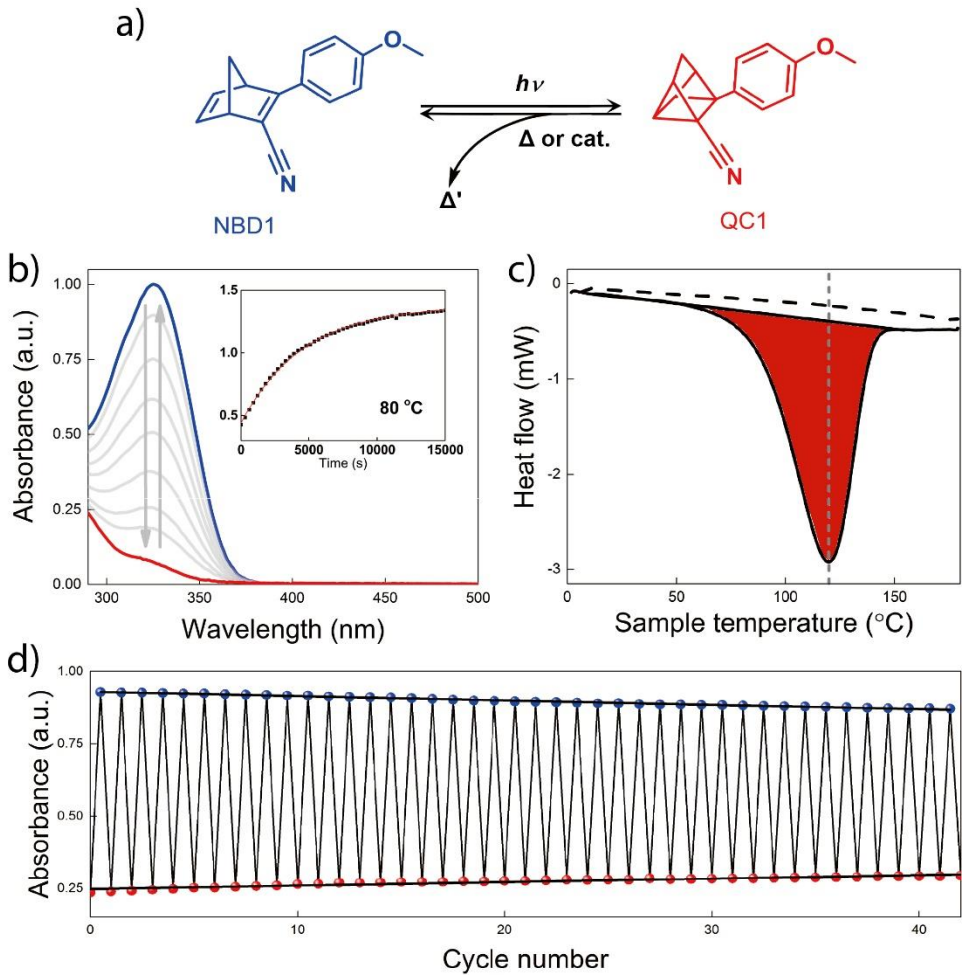

Figure 5.1. a) Structure and reaction scheme for **NBD1** and **QC1**; **b)** Absorption spectra of **NBD1** (in blue) and its photoisomer, **QC1** (in red). The sample was irradiated with a λ = 310 nm LED light. The inset figure shows the kinetic back-conversion of **QC1** under 80 °C; **c)** A DSC thermogram for **QC1** conversion to **NBD1**, ($\Delta H_{storage}$ = 89 kJ mol^{-1} was based on an average of two measurements). The dashed line shows the second run after heat release; **d)** Cyclability experiment for a solution of 0.7 x 10^{-4} M in toluene showing absorbance of **NBD1** in blue dots and **QC1** in red dots at λ = 325 nm. The black line indicates the degradation of 0.14% per cycle over 43 cycles. *© Reproduced with permission from the Royal Society of Chemistry.*

For an ideal MOST system, the material should be able to charge and discharge over an infinite number of cycles. Therefore, a cyclability test of **NBD1** was performed. The setup was based on a UV-Vis spectrophotometer as described in Chapter 4, section 4.5. A temperature tunable sample holder was installed inside the spectrophotometer, together with a time delay controllable LED light source (325 nm) which has been programmed to irradiate the sample at defined time intervals. It was found that in toluene, with a concentration of 0.7 x 10^{-4} M, the degradation rate was calculated as only 0.14% per cycle, affirming somewhat good robustness of the system (Figure 5.1d). Speculatively, the degradation could be the formation of dimerization through the unsubstituted olefin side of **NBD1**, however, due to the extreme diluted solution used for cycling test, it is hard to verify by NMR or other techniques.

5.3 Device conversion demonstration

After fully characterizing the MOST performance, **NBD1** was tested into an outdoor testing device (see Figure 5.2). This construction consisted of a parabolic concentrator combined with a solar tracker (with a net surface of 27.3 x 32.7 cm^2). Sunlight was focused on an apparatus where a double jacketed glass tube was located. It is noteworthy to mention that under a high flux of concentrated solar irradiation, the light focus point's temperature can potentially damage or even thermally back convert metastable molecules. To address this technicality, this double-layered glass tube was custom-made. The inner tube allows for flowing water to cool down the outer layer (5.8 mL with a pathlength of 1 mm), where the MOST solution flows. Theoretically, a saturated solution of **NBD1** can attend a maximum energy storage efficiency of 0.51%. (See Equation 4-22)

An **NBD1** solution of 4 mM in toluene was pumped through the outer layer of the glass tubing using different residence times which were inversely proportional to the average time that the solution is exposed to sunlight. The absorption spectrum before and after irradiation were recorded with a portable flow UV-Vis spectrophotometer. This experiment was performed on the 4th of May, 2016, on a sunny day in Gothenburg, Sweden. Theoretically for such concentration, the estimated maximum energy storage efficiency can

be reached to 0.20%. However, the highest measured energy storage efficiency was only 0.03%, with a conversion percentage of 64%.

Such a low energy storage efficiency could be attributed to the low compatibility of **NBD1** absorption spectra with the solar spectrum, thus wasting most of the incoming photons. For an ideal MOST device, the energy storage efficiency should change linearly with residence time before a full conversion.

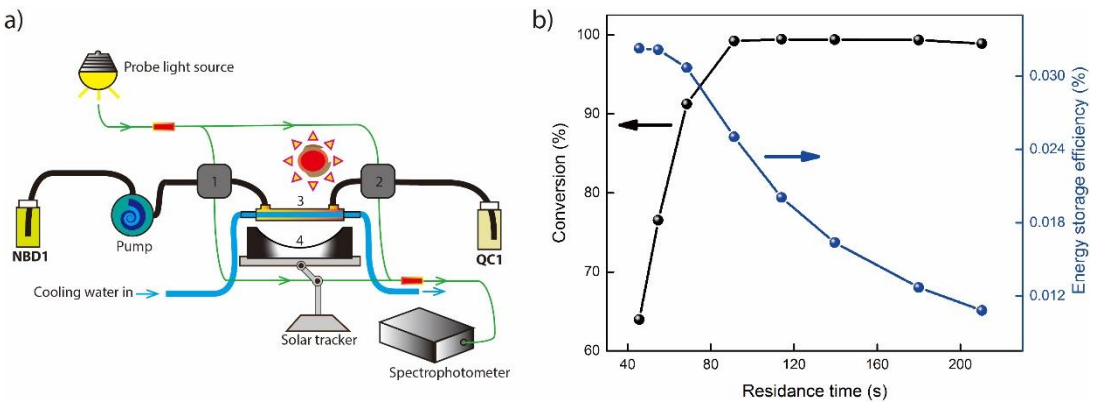

Figure 5.2. a) Outdoor solar tracker setup. Box 1 and 2 show the flow spectrometer, while device 3 represents a double-layered glass flow cell. The inner layer serves to pass through cooling water and the outer layer serves to flow **NBD1** solution. Device 4 shows a custom-made solar tracker; b) Conversion percentage (black) and energy storage efficiency (blue) varies with residence time for outdoor tests. *© Reproduced with permission from the Royal Society of Chemistry.*

5.4 Catalyst discovery, NMR studies and reaction rate determinations

Molecular design for long half-lives is necessary for energy storage purposes, however harnessing this energy is impractical when demand for the released energy is needed over a relatively short period. This issue can be circumvented by the use of a rapid back-conversion driven catalyst. Moreover, since MOST system should ideally be in liquid form, therefore, an efficient, heterogeneous catalyst is necessary to release “on-demand” the stored energy.[28] Various types of catalysts have been proposed for the back-conversion of QC and QC derivatives including rare metal-based salts and metal complexes.[111, 169, 170] In this thesis, 14 different heavy metal complexes and inorganic salts with transition metals, such

as Cu, Co, Pd, have been assayed initially with ^{1}H NMR, measuring in a rough way whether the catalyst candidate has any effect on **QC1**. These qualitative tests consisted of various NMR experiments. A solution of **NBD1** in $CDCl_3$ or toluene-d_8 was subjected to irradiation using a 310 nm LED lamp and monitored by ^{1}H NMR until complete **QC1** formation had occurred. At this point, a few milligrams of either the metal salt or complex was added to the tube. Around few minutes or half an hour later, progress of the back reaction is further monitored by ^{1}H NMR again.

Meanwhile, to quantify the rate of the potential catalyst, a 160 mL **NBD1** solution of 7.52 x 10^{-5} M in toluene ($A(\lambda_{max})$ = 1) was prepared. For each catalyst candidate, 2.5 mL of the solution was transferred to a 1 cm pathlength cuvette and irradiated until fully converted to **QC1**. A catalyst candidate was then added to the solution and the absorption change was recorded by a UV-Vis spectrometer at 347 nm over one hour. Later to calculate catalyst rate, the catalyst candidates are all considered as completely dissolved in toluene, assuming the back-conversion rate curve follows pseudo-first-order kinetics. With those two approximations in mind, a detailed list of catalytic performances can be found in table 5.2.

In order to avoid any purification steps after each heat release cycle, the selected catalyst should be insoluble in the functioning solvent, i.e., the catalyst should be heterogeneous, thus essential for a working device that can undergo multiple operating cycles. Interestingly, Co-based metal complex, cobalt (II) phthalocyanine (CoPc), showed a promising catalytic rate to trigger the **QC1** molecules back to **NBD1** (172 s^{-1} M^{-1}). Unfortunately, Ghani et al. determined that CoPc exhibited a low solubility in toluene, indicating that CoPc can potentially poison the liquid MOST and prevent or interfere with multiple cycling of the photoswitch couple.[171] Therefore, if CoPc is to be used as a catalyst, it needs to be fixed to a support that prevents potential leaching of the complex into a toluene solution containing **NBD1**. However, modifying CoPc with anchoring groups might affect the catalytic activity of the complex. In fact, the complex is a large polycyclic flat molecule which is capable of π-stacking, this can then be exploited by stacking onto insoluble support such as activated carbon by physisorption.

Table 5.2. Candidates of salts and transition metal complexes for the catalytic back-conversion of **QC1**. ✓ represents an active catalytic behavior by ^{1}H NMR, ✕ shows no obvious behavior of catalytic activation.

Number	Catalyst Name	Potential activity in $CDCl_3$	Potential activity in toluene	Reaction rate in toluene (s^{-1} M^{-1})
		Co(II)		
	CoPc	✓	✓	172,05
2	CoPc@C	✓	✓	11788,22
3	$Co(NO_3)_2 \cdot 6H_2O$	✕	✓	3,88
4	5,10,15,20-Tetrakis(4-methoxyphenyl)-21H,23H-porphine cobalt(II)	✕	✓	Dissolve in toluene and spectral overlap with NBD1, hard to follow by UV-Vis.
		Cu(I)		
5	CuBr	Degradation	✓	2,41
6	CuI	✕	✓	8,73
7	CuCN	✓	✓	4,09
8	$[Cu(CH_3CN)_4]PF_6$	Degradation	/	/
8*	$[Cu(CH_3CN)_4]PF_6$ + Butylated hydroxytoluene	Low degradation	/	/
		Cu(II)		
9	$CuCl_2$	Degradation	✓	2,52
10	$CuCl_2 \cdot 2H_2O$	Degradation	✕	0,03
11	$CuSO_4$	✓	✓	6,07
12	$(CH_3COO)_2Cu$	✓	✓	0,02
13	$(CH_3COO)_2Cu \cdot H_2O$	✓	✓	32,39
		Pd(II)		
14	$PdCl_2$	✓	✓	3,62
15	$(CH_3COO)_2Pd$	✓	✓	Slowly dissolve in toluene and spectral overlap with NBD1, hard to follow by UV-Vis.

Experimentally, CoPc was dissolved firstly in THF, then activated carbon was added and stirred over one week under Argon gas. The suspension solution was then centrifuged and washed a few times with toluene until no CoPc seems to be removed in solution. Later, it was found in macroscopic heat release experiments that leaking of CoPc from the support is caused by residual unremoved THF. Therefore, the powder was then dried to completely remove stacked THF molecules. To check the loading percentage of CoPc on carbon particles, XPS measurements were performed. It was finally calculated that around 13% of CoPc have been successfully adsorbed on the surface of activated carbon.

A UV-Vis scaled photoswitchable compound solution (ca. 10^{-5} M) was prepared. For each catalyst candidate, 2.5 mL of the solution was transferred to a cuvette with a 1 cm pathlength and irradiated until a full conversion is obtained. A potential catalyst (ca. 0.5 mg) was then added to the solution and the progressive absorption change was recorded by a UV-Vis spectrophotometer at a specific wavelength for at least one hour.

Surprisingly, the determined catalytic rate for the back-conversion of **QC1** to **NBD1** using this 13% loaded CoPc@C increased to 11.8 x 10^3 s^{-1} M^{-1}, which corresponded to a 69 time higher rate compared to pristine CoPc. This observation can be explained by the increase in relative surface area of active catalyst CoPc distributed over the surface of the carbon, as it's possible that CoPc can otherwise form intermolecular π-stacking aggregates thus blocking more of the active sites.

To confirm this hypothesis, Scanning Electron Microscope (SEM) images were obtained. From the SEM picture of the used pure activated carbon with 100 mesh (see Figure 5.3), it can be seen the carbon pieces are uniform, while, at the same time, containing big holes which can enlarge the surface area. However, no obvious aggregation of CoPc was observed on the CoPc@C SEM images, thus confirming the CoPc@C contains a very large reaction surface, potentially a very good sample for further macroscopic heat release demonstration.

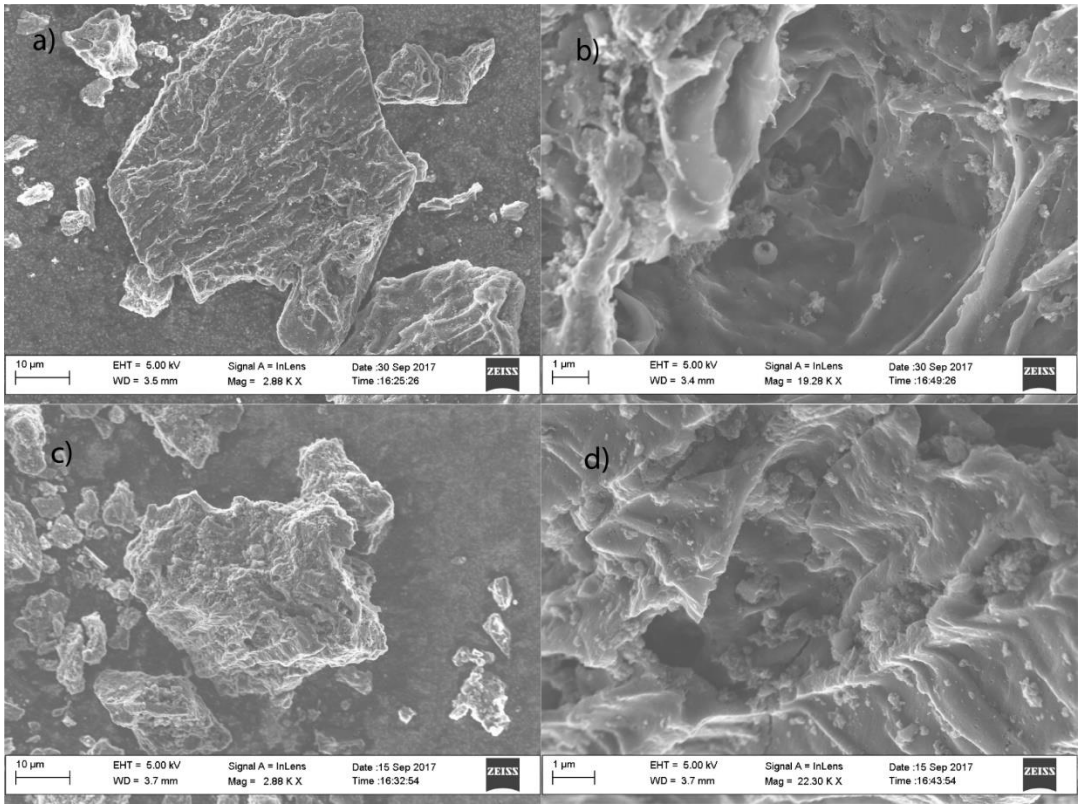

Figure 5.3. SEM images of: a) low magnification image of activated carbon; b) higher magnification image of activated carbon; c) low magnification image of CoPc@C; d) higher low magnification image of CoPc@C. *© Reproduced with permission from the Royal Society of Chemistry.*

5.5 Vacuum catalytic reaction chamber and macroscopic heat release demonstration

Previously, the energy density of **NBD1** was determined by DSC measurements, it is also important to measure in a macroscopic way the heat release from **QC1** when exposed to the heterogeneous catalyst. To practically make this catalyst reaction center, CoPc@C was packed into a Teflon tube (1.27 mm inner diameter, Cole-Parmer Instrument Company) with cotton blocking each side. When a charged **QC1** solution passes through the center, a temperature difference before and after the catalyst part can be measured with

thermocouples. However, it should be noted that, even with a low conductivity of the Teflon tube, convection heat loss from the reaction center to its surrounding area can still be a major problem. Based on this issue, the use of a vacuum chamber was necessary to minimize this energy dissipation to get more reliable values for the heat release process.

Connected to a turbo pump, this vacuum chamber can experimentally lower the inner pressure down to ca. 10^{-5} mbar. A schematic illustration of the experimental setup can be found in figure 5.4.

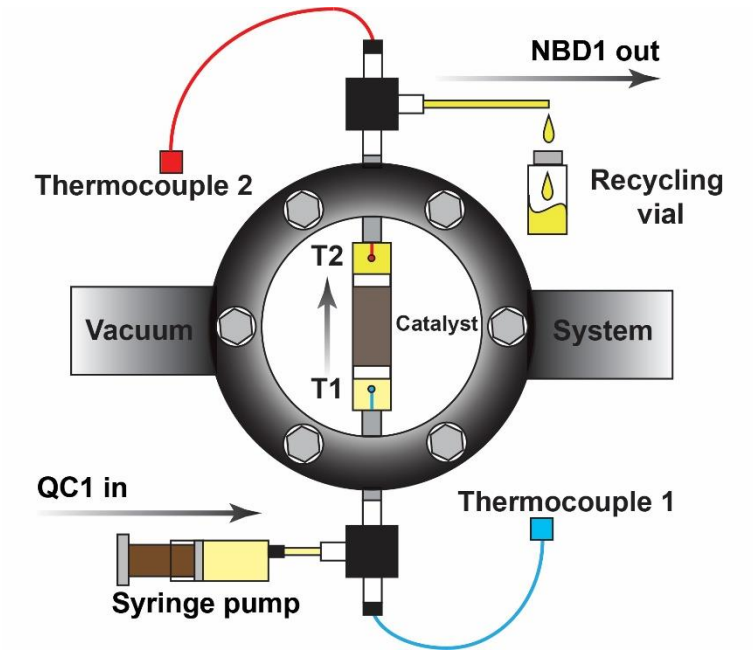

Figure 5.4. Illustration of the vacuum chamber. *© Reproduced with permission from the Royal Society of Chemistry.*

Meanwhile, for the purpose of obtaining the highest possible macroscopic heat release form the liquid MOST, the maximum solubility of **NBD1** in toluene need to be measured. It was determined that the solubility of **NBD1** in toluene can be reached to 1.52 M. Thus, the heat release temperature gradient vs. concentration is predicted in Figure 5.5, gray curve. It can be seen from Chapter 4, section 4.7, simulation method that, for a saturated solution, the theoretical maximum temperature difference can be as high as 66 °C, by considering the same specific heat capacity of **QC1** as unsubstituted QC, which equals to 1.66 J g^{-1} K^{-1}.

To experimentally quantify the macroscopic heat release, five solutions with different concentrations of **NBD1** in toluene from 0.10 M to 1.50 M were prepared and fully converted to **QC1** form under irradiation. It should be noticed that at low concentrations such as UV-Vis scale (ca. 10^{-5} M), the absorption of **QC1** can be more or less disregarded. However, at higher concentrations of the photoswitch couple, the inner filter effect can be largely amplified, such that when the concentration of **NBD1** is increased, the accumulating **QC1** can make a significant impact. With this issue in mind, all prepared **QC1** solutions were firstly prepared at high dilution in toluene and irradiated until a full conversion was obtained, then carefully concentrated to the desired concentration.

Meanwhile, the catalytic reaction center was loaded with ca. 5 mg of CoPc@C, then placed under high vacuum. When the vacuum pressure reached 10^{-5} mbar, the **QC1** solution was injected into the CoPc@C contained reactor with a flow speed of 5 mL h^{-1}. Compared to the predicted values, the measured temperature differences (blue and red dots in Figure 5.5) fit very well with the simulation. Much to the delight, a maximum temperature difference of 63.4 °C (an absolute temperature of 83.4 °C) from the 1.50 M charged **NBD1** solution was obtained, thus demonstrated a full functioning cycle of **NBD1** based MOST system from energy capture, energy storage and energy release.

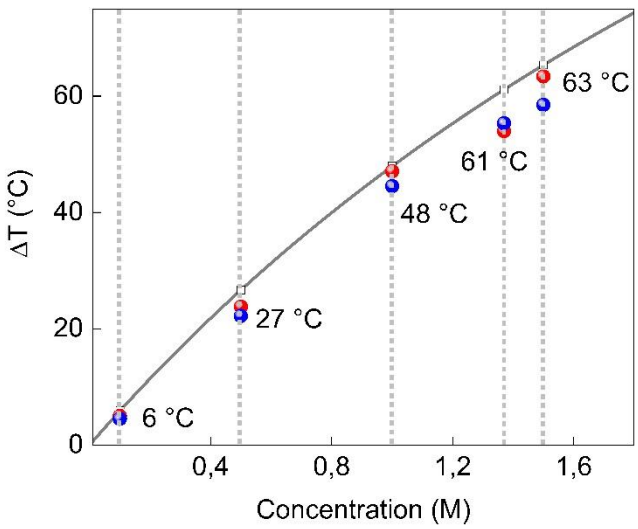

Figure 5.5. Theoretical simulation (grey line) and experimental data (blue dots for first measurement and red dot for the second measurement) of heat release vs. concentration. *© Reproduced with permission from the Royal Society of Chemistry.*

Unfortunately, it was found that the CoPc molecules cannot be fixed tightly on the activated carbon support while using a concentration higher than 0.10 M. The catalyst was observed to leak into the solution inflow, thus stopping the heat generation (see Figure 5.6).

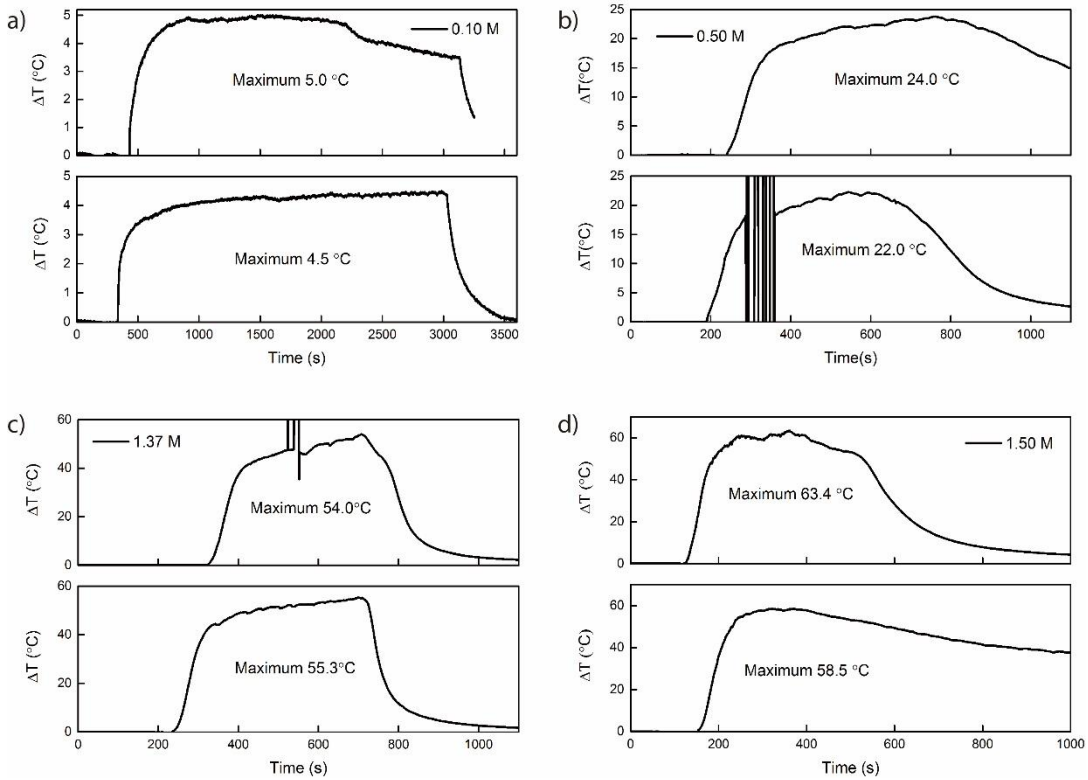

Figure 5.6. a) to d) show the heat released from 0.1 M to 1.5M concentrate samples. Each concentration was repeated once to confirm the final results. *© Reproduced from the Royal Society of Chemistry.*

With equations 4-26 and 4-27 from Chapter 4, a minimum TON of 482 and a TOF of 2.0 s^{-1} was determined for the ability of CoPc@C to convert **QC1** to **NBD1** in toluene. To put this into perspective, these values are far lower than the capabilities found for a typical enzyme such as carbonic anhydrase, which has a TOF of 4 x 10^5 ~ 6 x 10^5 s^{-1}. Certainly, more stable support for CoPc, or anchoring CoPc on fixed support with covalent bonds is unquestionably necessary, if this type of technology is to be used in a device capable of multiple cycling.

To further determine the effect of the leached CoPc on the ϕ_{iso} of **NBD1** conversion, the blue colored solution just after the reaction center was collected, appropriately diluted and

remeasured the ϕ_{iso}. It was found that the blue color of the metal complex faded gradually over time to yellow under ambient conditions, very likely due to the catalytic activity loss of the metallated phthalocyanine. This observation was later confirmed by detailed quantum yield measurements. In any case, the freshly collected blue solution showed an approximate 4% decrease in quantum yield compared to that of the pure **NBD1** solution. In addition, after 11h, the absorption at 364 nm was observed to be increased, confirming that this dissolved CoPc contaminant still had a catalytic effect on back-converting **QC1** molecules in solution. After 3 days, when the solution changed its color completely to yellow, its quantum yield for the photoconversion of **NBD1** returned back to original 61%. A ^{1}H NMR spectrum was also taken, where no degradation of **NBD1** was observed. (see Figure 5.7)

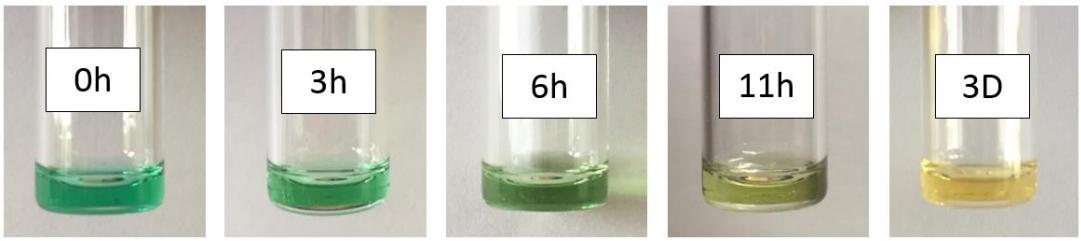

Figure 5.7. Color changes of **NBD1** solution with depleted catalyst over time. (photo from left to right: 0 hour, 3 hours, 6 hours, 11 hours, 3 days) *© Reproduced with permission from the Royal Society of Chemistry.*

5.6 Theoretical calculations of the back-conversion mechanism

To understand in detail how the CoPc worked for **QC1** molecules, a detailed DFT calculation was also performed at La Rojia University, Spain. In brief, Co(II) ion is presumably coordinated with **QC1** molecule, proceeding via various transition states en route back to **NBD1** form. Therefore, all possible transition states of the energy landscape have been proposed, including energy changes caused by positions or orientations of D-A substituents relative to the catalyst. Thus, a full catalyst reaction route has been proposed in figure 5.8 in an attempt to rationalize experimental observations.

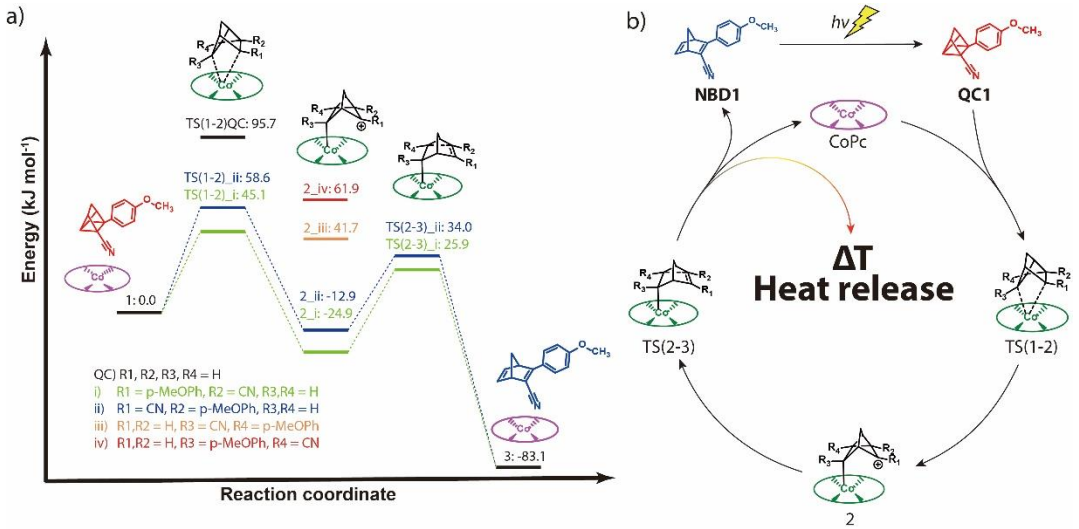

Figure 5.8. a) Critical points along the potential energy surface for the catalytic reaction conversion of **QC1** to **NBD1** using CoPc (free energies in kJ mol^{-1} computed in toluene referred to a 10 Å separation of CoPc and **QC1**). The color coding represents molecular structures or orientations. **b)** Catalytic cycle for the back-reaction. *© Reproduced with permission from the Royal Society of Chemistry.*

5.7 Modification of the push-pull NBD for extending the conjugation through donor-acceptor (D-A)

As mentioned earlier, the extension of the π-conjugation system typically redshifts the absorption spectrum of the molecule, due to the lowering of the HOMO-LOMO gap of the molecule. This lowers the energy needed for excitation, but more importantly, this can be used to better align the absorption of a photoswitch with the solar spectrum.[113, 172] As **NBD1** can be easily synthesized on large scale, this provides an opportunity to make new derivatives based on **NBD1**, specifically, extending the conjugation along the D-A chain.

Conveniently, **NBD1** possesses a cyano-group which can undergo further functionalization. With this in mind, the nitrile group of **NBD1** was therefore reduced to the aldehyde by the treatment of **NBD1** with diisobutylaluminiumhydride (DIBALH), affording **NBD2**. The reactive nature of the aldehyde moiety could be taken advantage of where **NBD2** could be treated with both a phosphonate ester (1) for a Horner-Wadsworth-Emmons olefination

forming *E/Z*-**NBD3**, and stabilized phosphorane (2) for a Wittig reaction forming *E*-**NBD4** (see Scheme 5.3). In both these cases nitrile and ester acceptors have been introduced while at the same time extending the conjugation by one olefin.

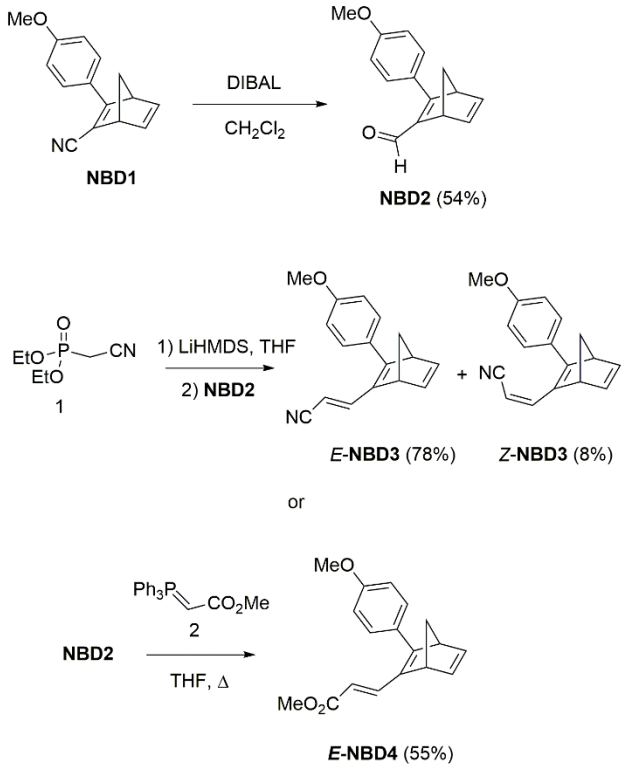

Scheme 5.3. Reduction of **NBD1** giving NBD2 and subsequent reactions to extend conjugation from the 2-position to form *E/Z*-**NBD3** and *E*-**NBD4**.

All these new molecules were examined for their suitability for MOST. Spectroscopically, the onset of absorption for the aldehyde derivative, **NBD2**, was found to be slightly red-shifted compared to **NBD1**.

For the π-extended derivatives *E*-**NBD3** and *E*-**NBD4** a larger degree of redshifting of the absorption spectrum was observed. In fact, the latter exhibited an absorption onset of 427 nm in toluene. However, it was found that metastable *E*-**QC3** and *E*-**QC4** exhibited extremely short lifetimes of only minutes in toluene. As expected, the half-life of *E*-**QC4** was measured to be longer than that of *E*-**QC3**, since this is a common challenge to overcome in MOST,

where redshifting the absorbance of an NBD typically is associated with decrease in half-life. (see Table. 5.3).

Table 5.3. UV-vis spectral data and kinetic data for NBDs and corresponding QCs in toluene. [a] It was not possible to measure quantum yields and onsets for purified *E*-**QC3** and *E*-**QC4** due to their short half-lives.

NBD	λ_{max} (nm)	λ_{onset} (nm)	Φ_{iso} (%)	**QC**	λ_{onset} (nm)	Spectral window (nm)	$\Delta H^{\ddagger}_{therm}$ (kJ mol^{-1})	$\Delta S^{\ddagger}$ (J mol^{-1} K^{-1})	$\Delta G^{\ddagger}$ (kJ mol^{-1})	$t_{1/2\ @\ 25\ °C}$
1	326	380	61	**1**	345	35	103,8	-22,4	110,5	30 days
2	332	408	78	**2**	382	26	71,9	-101,6	102,3	25.4 hours
E -**NBD3**	355	419	-[a]	*E* -**QC3**	-[a]	-	59,4	-83,3	84,2	1.0 min
E -**NBD4**	356	427	-[a]	*E* -**QC4**	-[a]	-	75,6	-48,6	86,1	2.4 min

To summarize, the modifications of **NBD1** by extending the π-conjugation can give derivatives with a relative red shifting of the onset of absorption. However, at the same time, the energy storage half-life of these derivatives were drastically affected by such modifications. At the same time this work was being undertaken, efforts were made to place bulky substituents to the C7 position of **NBD1** (see Scheme 5.4) and, in this cases, the energy storage half-life has been significantly increased, confirming previous observations of bulkier groups stabilizing the QC form, however in these cases the 7 position substitution does not afford a redshift in absorption for the new derivatives. [116]

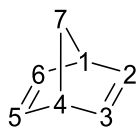

Numbered carbon positions for a NBD molecule

Scheme 5.4. Numbered carbon positions for an NBD molecule (C1 to C7, olefins locate through C2-C3 and C6-C7).

Chapter 6

Other photoswitches for MOST

*In this chapter, two other MOST candidates including an AZO derivative and **DHA1** photoswitches were characterized in detail. The two systems were later integrated into devices for full MOST evaluations. (paper III, IV).*

6.1 Azobenzene derivative

6.1.1 Introduction

As a potential MOST candidate, azobenzenes (AZO) have been in the spotlight over the last few decades because of its broad optical absorption, robustness, and storage lifetime as well as its tunable energy storage density.[31] Unsubstituted azobenzene has been determined to have an energy storage density of 50 kJ mol^{-1} with a photoisomerization quantum yield of 45%.[31, 90, 103] It has even been integrated into a device for evaluating its MOST efficiency.[94] However, the compound is not suitable for solar energy storage because of the high efficiency of the photon-induced back-conversion from *cis* to *trans* state, therefore forming a photostationary state after a long periods of irradiation, where the conversion and back-conversion process turned into an equilibrium over irradiation.[94, 104] Thus, various efforts have been made to improve the molecular behavior by modifying the substituents to separate the absorption profiles between *cis* and *trans* isomers.[31]

One of the improved samples was synthesized by K. Masutani, M. Morikawa and N. Kimizuka, whereby adding a branched 2-ethylhexyloxy group, resulted in the formation of a liquid azobenzene derivative(**AZO1**, see Figure 6.1a).[102] As mentioned in Chapter 2, this liquid form

photoswitch could potentially be a promising candidate for MOST applications in device. Moreover, the measured energy storage density of this **AZO1** is equal to 52 kJ mol^{-1}, which can potentially fulfill MOST requirements. Therefore, further characterization was performed, with the goal of incorporation into a device in order to achieve the first demonstration of an azobenzene derivative for a lab-scale test.

6.1.2 Characterization of the materials

Previously, it was reported that azobenzene derivatives behave differently in solvents with different polarities,[102] therefore, to be able to compare the MOST performance with NBD derivatives as well as dihydroazulene derivative (**DHA1**) later in this chapter, toluene was chosen as the working solvent for all characterization and device tests in this thesis.

Spectroscopically, the onset absorption of **AZO1**-*trans* is located at 513 nm ($\varepsilon_{@513\ nm}$ > 100 $M^{-1}\ cm^{-1}$, λ_{max} = 350 nm, $\varepsilon_{350\ nm}$ = 2.5 x 10^4 $M^{-1}\ cm^{-1}$, see Figure 6.1b). However, the effective conversion wavelength remains below 400 nm, which can be assigned to π-π* absorptions. The converted *cis* form of **AZO1** can also absorb light. However, with photons from ca. 400 to 513 nm, which correspond to n-π* absorptions, it can actually photon-induced back convert the charged *cis* state (P-type back-conversion).[102] Therefore, in the end, both absorptions produce a photostationary state. In addition, it was observed that, at 340 nm, the conversion quantum yield was determined to equal 21%; conversely, at 455 nm, the photo-induced back-conversion quantum yield was equal to 23%, slightly higher than the conversion process. For further tests, a bandpass filter was used in all device conversion experiments to prevent the photo-driven back-conversion (thickness of 1 mm from SCHOTT, filters out all light above 400 nm).

Concerning half-life, as a nonpolar solvent, toluene gives the *cis* photoisomer a half-life of 36.3 h, which can potentially fulfill a daily storage period. From the Arrhenius equation, it was found that the activation energy E_a equaled 96 kJ mol^{-1}. The activation enthalpy could also be determined from the Eyring plot, giving values of $\Delta H^{\ddagger}_{therm}$ = 93.7 kJ mol^{-1}, together with an activation entropy $\Delta S^{\ddagger}_{therm}$ = -31.7 J $mol^{-1}\ K^{-1}$. (see Figure 6.1c)

A cyclability test was carried out using a diluted **AZO1** toluene solution (ca. 10^{-5} M). Two LED light sources with wavelengths of 340 nm (~60 mW, 100 s) and 455 nm (~1020 mW, 300 s) were irradiated alternatively to charge and discharge the solution. Experimentally, a solution of **AZO1** in toluene with ca. 10^{-5} M was prepared without degassing. The charge and discharge processes were achieved with a 340 nm LED (~60 mW) over 100 s and a 455 nm LED (~1020 mW) over 300 s, alternatively. The absorbance was monitored at 350 nm. Results showed that over 203 charging and optical discharging cycles, no degradation was observed, thus showing high stability of this photoswitch, even under aerobic environment. (see Figure 6.1d)

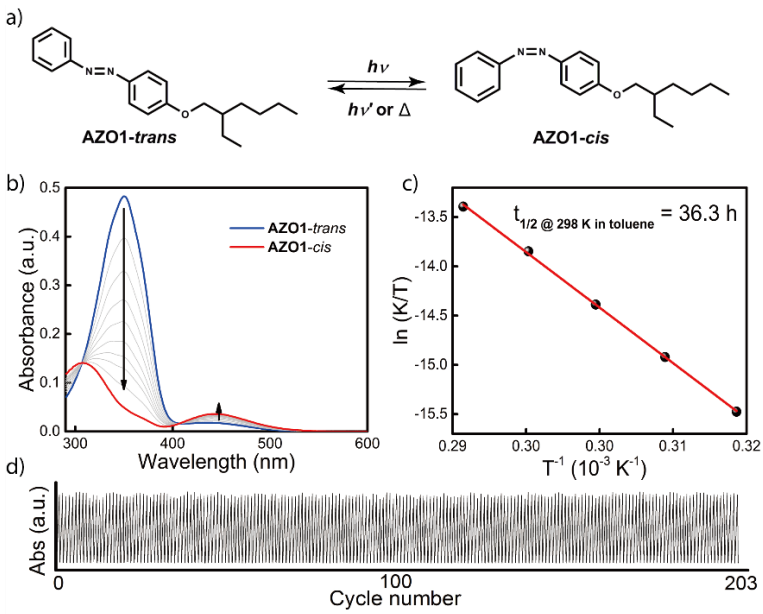

Figure 6.1. a) Structure of **AZO1** in *trans* and *cis* states. **b)** Absorption spectra of **AZO1** -*trans* (in blue) and its corresponding photoisomer in the *cis* state (in red). The sample (ca. 2 mg into 100 mL toluene) was converted with a 340 nm LED lamp. **c)** Eyring plot of **AZO1**-*cis*. The half-life at 25 °C was determined as 36.3 h in toluene solution. **d)** Optical cycling test of **AZO1** in toluene. The figure shows 203 cycles in total. *© Reproduced with permission from the Royal Society of Chemistry.*

6.1.3 Conversion device tests

In 1987, Taoda et al. tested unfunctionalized azobenzene in a device, however structurally modified azobenzene derivatives have never been integrated into devices.[94] Hence, a flow

system was built to further demonstrate the **AZO1** material in a lab-scale microfluidic chip under AM 1.5 simulated solar light. Two solutions with concentrations of 0.2 mM and 0.5 mM of **AZO1**-*trans* in toluene were prepared and passed through the microfluidic chip individually with different residence times. The microfluidic chip was customized with a channel depth of 100 µm, and a total volume of 33.9 mm^3. The conversion status was checked with a portable flow UV-Vis spectrometer. Since photo-induced back-conversion can happen while irradiating with a full solar spectrum, a bandpass filter (> 400 nm blocked) was inserted in between the solar simulator and microfluidic chip. The setup of such an experiment can be seen in figure 6.2a.

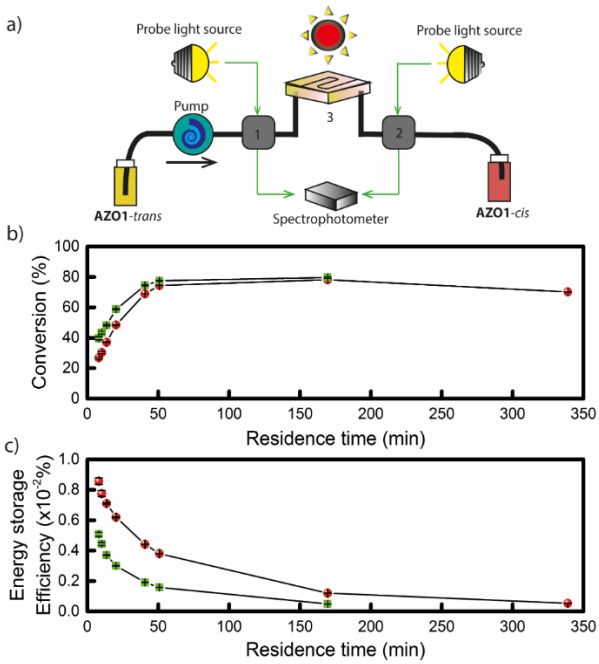

Figure 6.2. a) Experimental setup of **AZO1** in a fluidic chip device. Gray boxes 1 and 2 contain a flow UV-Vis detection device connected to a portable spectrophotometer. Device 3 corresponds to a total volume of 33.9 mm^3 quartz chip, with a 100-µm optical path length. **b)** Experimental data of two concentrations used: 2 x 10^{-4} M in green, and 5 x 10^{-4} M in red. Conversion percentage of **AZO1**-*trans* with different residence times in the microfluidic chip. **c)** Measured energy storage efficiency of the **AZO1** compound in toluene. *© Reproduced with permission from the Royal Society of Chemistry.*

To calculate the conversion percentage and energy storage efficiency, the isosbestic point can be used. This is a specific wavelength where the total absorbance of the sample solution does not change during a certain chemical, photophysical or photochemical reaction. Unlike

NBD compounds, the absorption spectrum of the **AZO1**-*cis* state has an overlap with its *trans* state. Therefore, a conversion percentage formula can be used with the help of isosbestic points. Hence, the conversion percentage and energy storage efficiency can be calculated using the method described in chapter 4, section 4.8 of this thesis.

Theoretically, without a photo-induced filter, the maximum energy storage efficiency was calculated to be 2.6%. However, in order to avoid photo back conversion, a filter that can cut off all incident photons above 400 nm would be needed. Therefore, using equation 4-23, it was determined that the maximum energy storage efficiency for a neat sample was estimated to be 0.88%. For a concentration of 0.5 mM and 0.2 mM, the efficiencies were expected to be as high as 0.02% and 0.01%, respectively.

Experimentally, the actual measurements are shown in Figure 6.2b, c. It was found that a maximum conversion of only 79% forming the metastable isomers can only be achieved, even with a diluted sample of 0.2 mM. This was very likely due to the photo-stationary state between the two **AZO1** isomers. The maximum storage efficiency was, however, determined to be 0.009% and 0.005% for 0.5 mM and 0.2 mM, respectively. It seems that a huge efficiency loss was observed, likely due to complications coming about from the photostationary state between the two isomers. Since **AZO1** can be back-converted by visible light (P-type back-conversion), the outdoor test for this system was not performed.

6.1.4 Catalytic back-conversion in device

To further estimate the maximum energy that a fully charged **AZO1** solution can release, the theoretical maximum temperature was estimated with a more accurate equation 4-15 from chapter 4, specifically for neat sample. As result, assuming a neat 100% converted **AZO1** sample was used, the estimated maximum temperature increase was determined to be ca. 226 °C.

Regarding the facilitation of the back-conversion, various catalysts have been previously investigated, which included electrocatalytic methods,[173] gold nanoparticles that can perform redox reactions,[174] as well as several mineral acids, such as perchloric acid[175] and Cu(II) salts[176]. For a closed operating system, a heterogeneous form catalyst akin to CoPc@C

used with the **QC1** system which can be fixed in a reaction center was certainly needed. Since the solvent used in these studies was toluene, in which the previously used CoPc@C and $[Cu(CH_3CN)_4]PF_6$ exhibited a very low solubility, it was thought that these transition metal-containing entities could be integrated into a Teflon tube as catalyst reactors, individually. Firstly, since CoPc had been previously found to have catalytic effect on AZO molecules,[94] only $[Cu(CH_3CN)_4]PF_6$ was mixed with a pre-converted **AZO1**-*cis* solution in toluene-d_8 (molar ratio as **AZO1**-*cis*: $[Cu(CH_3CN)_4]PF_6$ = 2:1 in toluene). After 1 h and 30 mins, a full back-conversion from **AZO1**-*cis* to **AZO1**-*trans* has been successfully observed via ^{1}H NMR spectrum, showing a positive catalytic effect of on **AZO1** molecules. Then, the corresponding back-conversion rates were determined via UV-Vis spectroscopy, this was done by adding the transition metal directly to a converted *cis* isomer solution in a cuvette (0.5 mM **AZO1** in toluene, 79% conversion from *trans* to *cis* state accomplished). As calculated, the back-conversion rate was fitted to 30 s^{-1} and 131.9 s^{-1} for $[Cu(CH_3CN)_4]PF_6$ and CoPc@C, respectively. Additionally, CoPc@C was still observed to have a slight leaking effect in toluene, thus it was decided that $[Cu(CH_3CN)_4]PF_6$ would be incorporated as the catalytic device for the flow reactor. 5 mg of this Cu(I) salt was inserted into a 5 cm long, 1 mm inner diameter Teflon tube (see Figure 6.3). With 1 mL h^{-1} flow speed, a 0.5 mM solution of 79% AZO *cis* solution was passed through the reaction center. This resulted in 48% of the converted *cis* state which was successfully back converted to its initial *trans* state.

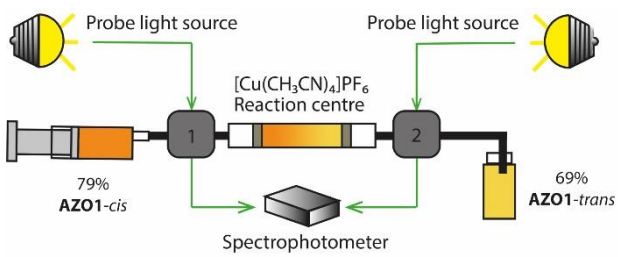

Figure 6.3. Conceptual device demonstration of the catalytic back-conversion of **AZO1**-*cis*. Around 5 mg of Cu(I) salt was loaded into the reaction center. A 0.5 mM 79% **AZO1**-*cis* solution was flown through the Cu(I) reactor with a speed of 1 mL h^{-1}. 69% of the **AZO1**-*trans* was obtained after the reaction center, i.e. 48% of the **AZO1**-*cis* can be successfully back converted to **AZO1**-*trans* state. *© Reproduced with permission from the Royal Society of Chemistry.*

To further investigate the fundamental functioning mechanism of Cu(I) salt on **AZO1**-*cis*, DFT calculations were performed at La Rojia University in Spain. In brief, it was found that in the presence of Cu(I), the reaction barrier can be decreased by 4 orders of magnitude, thus

lowering the energy barrier and consequently accelerating the back-conversion process of the *cis* state.

6.1.5 Conclusion

In this part, an **AZO1** based MOST system has been successfully demonstrated, including molecule charging and discharging. Compared to unsubstituted azobenzene, **AZO1** *trans*-state did not exhibit a significant spectral shift. However, it still features a strong absorption ($\varepsilon_{max@350\ nm}$ = 2.6 x 10^4 M^{-1} cm^{-1}) and a long half-life ($t_{1/2}$ = 36.3 h at room temperature) in toluene. The cycling tests showed very high stability for the **AZO1** as no significant degradation was observed over 203 optical charge and discharge cycles. Some drawbacks still remain for its use for MOST purposes, such as a low quantum yield for conversion reaction above 340 nm and a photostationary state caused by the photoinduced back-conversion around 455 nm. Concerning energy storage, it can be predicted that with a bandpass filter below 400 nm, the simulated maximum energy storage efficiency for a neat sample can reach 0.88%. However, as neat **AZO1** samples cannot be completely converted to pure *cis* state, two solutions of 0.2 mM and 0.5 mM were prepared for testing. The calculated maximum energy storage efficiency was equal to 0.02% and 0.01%, respectively. Experimentally, with a flow system, efficiencies of 0.005% and 0.009% were finally measured. To further investigate the catalytic back conversion, it can be calculated that the fully charged neat sample can theoretically release 226 °C. Finally, $[Cu(CH_3CN)_4]PF_6$ salt was identified as an efficient catalyst and then integrated as a reaction center in the Teflon tube. At 0.5 mM, 48% of the *cis* state can be successfully back converted to *trans* state when using a flow speed of 1 mL h^{-1}, however, this conversion rate and flow speed are still too slow to be used for a macroscopic heat release experiment, even under vacuum due to low catalyst rate of the used Cu(I) salt. Finally, a DFT calculation was performed to determine the functioning mechanism of the Cu(I) salt. This discovery could help future catalyst design for all different types of azobenzene-based MOST systems.

Even though the work showed a complete charge and discharge azobenzene derivatives-based MOST demonstration, just like what J. Olmsted et al. claimed, it can still be concluded that azobenzene is not favored for energy storage purpose.[104] However, such a system can

be combined chemically[93, 119] (fused to a single MOST molecule) or physically (solution mixture of different MOST candidates) with other MOST candidates in order to form a complement for each other's systems.

6.2 Dihydroazulene photochromic derivative

6.2.1 Introduction

In 1984, Daub et al. discovered a photoswitchable molecule that can undergo a 10π retrocyclization reaction, named the dihydroazulene derivative **DHA1** which converts to its corresponding vinylheptafulvene **VHF1** structure (see Scheme 6.1, where the **DHA1** shown is considered as the DHA-moiety).[133] The charged **VHF1**, itself, has two-states, however, the *trans*-state is thermaldynamically more stable. In fact, it needs to be in the *cis* form to adopt transition state for the back-conversion. As with QC derivatives, **VHF1** can later be thermally or catalytically back-converted to reform **DHA1** and therefore, molecules bearing this photochromic motif have been studied as possible candidates for MOST.[119, 140, 142, 143, 177] During recent decades, many DHA-based derivatives have been synthesized and characterized, however, a lab-scale MOST demonstration for DHA-derivatives has not been previously realized.

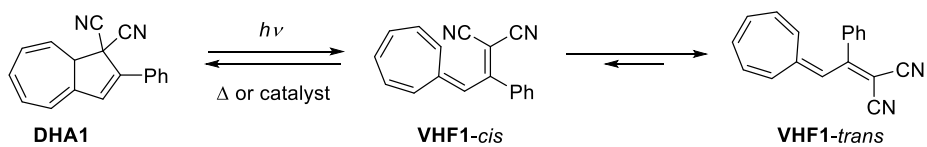

Scheme 6.1. Photoisomerization reaction of the dihydroazulene derivative (**DHA1**) and its corresponding vinylheptafulvene (**VHF1**) couple.

There are a few methods to synthesize **DHA1**. Early methods involved a key step of [8+2π] cycloaddition reaction, but this method did not translate well to large scale.[178] More detailed descriptions of the problem are beyond the scope of the thesis and will not be listed. In 2011, Broman et al. reported an alternate protocol for the formation of **DHA1**. This alteration translated to the possibility of a large scale synthesis, ca. 15 g.[138] Hence, as the first step approaching industrialization, in this thesis, **DHA1** was tested in devices for a detailed MOST demonstration.

6.2.2 Characterization of the materials

Due to the polarity differences between the parent and photoisomer state, it is known that **DHA1** behaves differently depending on the polarity of the solvent used.[138] Therefore, the functional solvent needs to be chosen wisely in order to simplify the integration into a practical MOST device. Thus, three potential solvents: toluene (relative polarity: 0.099), acetonitrile (relative polarity: 0.460) and ethanol (relative polarity: 0.654), with increasing polarity, were selected to cover a large polarity range (The values for relative polarity are normalized from measurements of solvent shifts of absorption spectra and were extracted from literature).[179] A comparison of the photoisomerization quantum yield, thermal back-conversion half-life, solubility as well as the degradation rate of **DHA1** in each of the three solvents can be found below in table 6.1.

Table 6.1. The physical properties of **DHA1** in different solvents. © *Reproduced with permission from ChemSusChem, John Wiley and Sons.*

Solvent	Photoisomerization quantum yield	Thermally-induced back-conversion half-life at 25 °C (min)	Solubility (mg mL^{-1})	Degradation (% loss per cycle)
Toluene	0,6	1474	55	0,01
Acetonitrile	0,55	218	36	0,18
Ethanol	0,5	202	5	0,21

Clearly, toluene is the most favorable solvent for further MOST demonstrations, because of the high photoisomerization quantum yield, long thermal half-life, high solubility and robust performance of the photon charge, thermal discharge cycling repetition. In addition, it was also found that only 0.01% degradation occurred after 70 cycles (see Figure 6.4a). The solutions in ethanol and acetonitrile were also analyzed with LC-MS after the cyclability tests, but many side products can be found, which were difficult to identify. In addition, the two polar solvents can help facilitate the elimination of hydrogen cyanide, the driving force being the formation of an aromatized azulene. When the cycling was carried out in ethanol, an ethanol adduct could also be identified. (see Figure 6.4b).

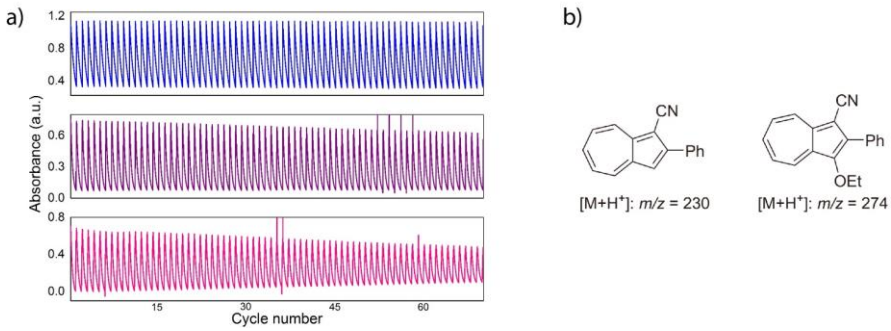

Figure 6.4. a) Cyclability test (concentration ca. 10^{-5} M for each case) for **DHA1/VHF1** based on absorbance at 460 nm in toluene (blue), acetonitrile (purple) and ethanol (red). The experiments were performed at a constant temperature of 60 °C during the experiments, in order to reduce the back-conversion time. Light at 365 nm was repeatedly switched on and off. One cycle corresponds to one *light-on* period and one *light-off* period. A total of 70 cycles are shown. The baseline absorption increase for the ethanol sample is potentially attributed to the formation of azulene. Parasitic signals (spikes) appear in acetonitrile and ethanol samples due to instrument fluctuations; b) Possible degradation products based on mass spectrometry analysis. *© Reproduced from ChemSusChem, John Wiley and Sons*.

It is worth mentioning that the onset of absorption for **DHA1** in toluene is positioned around 450 nm ($\varepsilon_{@450\ nm} > 100\ M^{-1}\ cm^{-1}$, λ_{max} = 360 nm, $\varepsilon_{350\ nm} = 1.6 \times 10^4\ M^{-1}\ cm^{-1}$, see Figure 6.5), indeed covering a part of the visible solar spectrum. However, as a positive photochromic material, like the absorptivity for the **AZO1**-*cis/trans* couple, the converted **VHF1** also has a spectral overlap with its corresponding photoisomer, **DHA1**. Therefore, a full conversion can hardly be achieved due to the shielded light from the increasing **VHF1** concentration throughout the conversion.

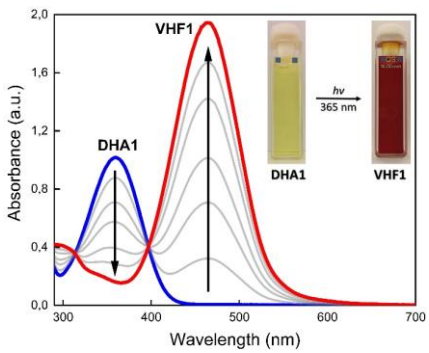

Figure 6.5: Absorption spectra of **DHA1** (in blue) and its photo-isomer **VHF1** (in red); insert shows color change of the compound in toluene before and after irradiation with 365 nm light. *© Reproduced with permission from ChemSusChem, John Wiley and Sons.*

With these preliminary results in mind, and for the convenience of comparing the results directly with **NBD1** and **AZO1**, toluene was selected as the device testing solvent for **DHA1**.

6.2.3 Conversion device tests

To demonstrate a DHA-based proof-of-principal concept, a commercial chip from Syrris Ltd (a total volume of 62.5 µL; contains an effective exposure volume of 35.72 µL, irradiation surface of 5.18 cm^2 and a channel depth of 85 µm), was used to establish the microfluidic conversion setup similar as the setup used in Section 6.1.3.

It was found that the calculated maximum energy storage efficiency that could be reached is 0.83%, with a spectrum cut-off wavelength of 454 nm under a simulated AM 1.5 solar light (0.81% under global AM 1.5 real sunlight). (See Figure 6.6)

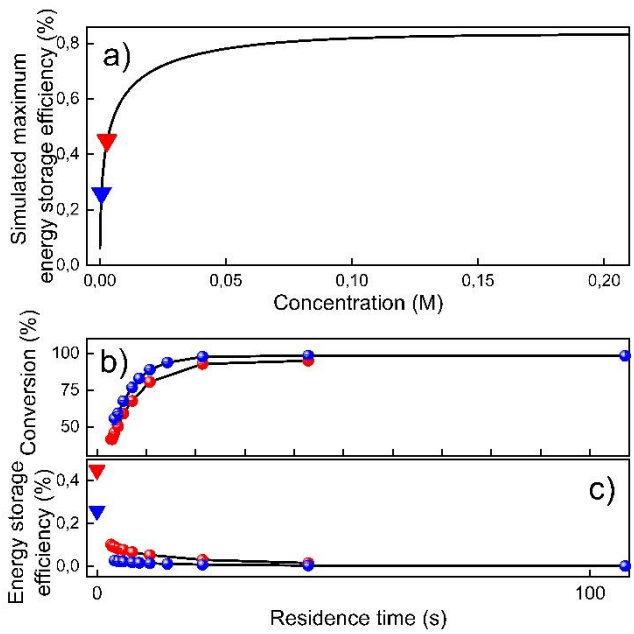

Figure 6.6: a) Simulated maximum energy storage efficiency varies with a concentration in commercial Syrris chip. The black line indicates the simulation of the efficiency under a simulated light source; b) Conversion percentage and measured energy storage efficiency vary with different residence times of the solution. Blue dots correspond to a concentration of 0.7 mM and red dots correspond to a concentration of 0.3 mM. *© Reproduced with permission from ChemSusChem, John Wiley and Sons.*

Experimentally, two concentrations with ca. 0.7 mM and 0.3 mM were prepared and stored in the dark. With different flow speeds, these two solutions were passed through the microfluidic chip, individually, to determine the conversion percentage and energy storage efficiency. In theory, for 0.7 mM and 0.3 mM, a theoretical limit of 0.26% and 0.45% can be calculated, respectively. The experimentally measured values were 0.03% and 0.10% with a residence time in the chip of 3.6 s and 2.9 s, respectively, approaching the expected values, however somewhat lower than the calculated values. In an ideal case, a good MOST system should show a linear dependence of energy storage efficiency *vs.* residence time. Conversely, in this case, the efficiency dropped significantly with increasing residence time, thus showing strong inner filtering effects due to accumulating **VHF1**, whose absorption competes with that of its parent molecule **DHA1**.

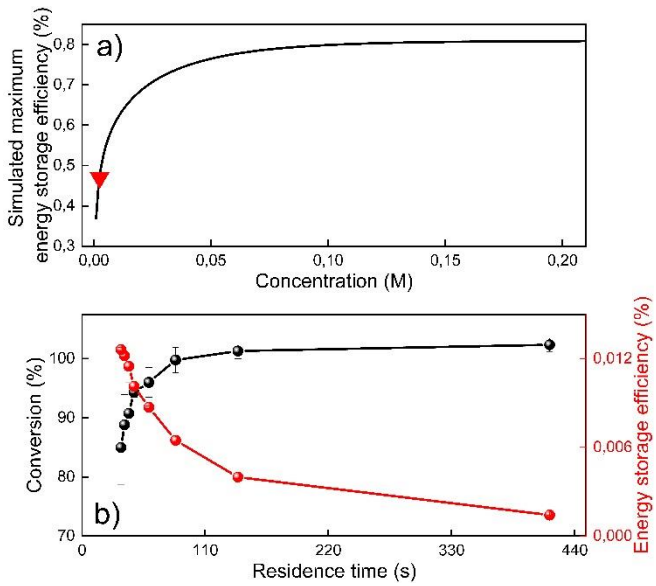

Figure 6.7. a) Maximum energy storage efficiency of the outdoor tests. The black line shows the results under a simulated solar lamp while the red line shows the efficiency under AM 1.5 global sunlight; b) Conversion percentage and energy storage efficiency for an outdoor test. Data were collected twice during one sunny day in Gothenburg, Sweden. *© Reproduced with permission from ChemSusChem, John Wiley and Sons.*

The evaluation of a DHA-based system has never been tested under outdoor conditions, and so, a large scale device demonstration could further determine where future efforts should be directed. Additionally, a large scale prototype is necessary to achieve a lab-to-site technical transfer. Therefore, the custom-made solar parabolic concentrator, which was

used for the **NBD1** system, was also used to test the **DHA1/VHF1** couple for its MOST performance. (see Figure 6.7)

Under direct sunlight, the maximum energy storage efficiency was limited to 0.81% as mentioned before, and therefore, a solution of 0.3 mM was tested on a sunny day, without clouds assuming to have solar irradiation of AM 1.5, in Gothenburg, Sweden. According to the results, 0.47% was the limited efficiency for this concentration. However, the real measurement only reached 0.013% efficiency, significantly lower than the predicted value. This huge efficiency loss was likely caused by the long pathlength of the collecting tube, which consequently wastes incoming photons, thus amplifying the complications coming about from inner filter effects.

6.2.4 Catalytic back-conversion in device

In previous research, Cu(I) ion source was found to be catalytically active for the back-conversion from **VHF1** to **DHA1**.[142] Yet, a device proof with efficient catalytic back-conversion had not been tested. Thus, $[Cu(CH_3CN_4)]BF_4$ was then integrated into a Teflon tube to form a reaction center. ca. 1 mM of the pre-converted **VHF1** solution was passed through the reaction center with a flow speed of 5 mL h^{-1}, and the concentration status was checked before and after the catalyst center with an inline UV-Vis spectrometer (See Figure 6.8, similar as in Section 6.1.4 for the back-conversion reaction of **AZO1**-*cis*).

This resulted in up to 81.3% back-conversion of **VHF1** to **DHA1**. Still, it needs to be mentioned that, at this concentration and conversion percentage, a macroscopic heat release demonstration like the case for **NBD1** could still not be achieved, and further investigation into a more efficient catalyst is certainly necessary.

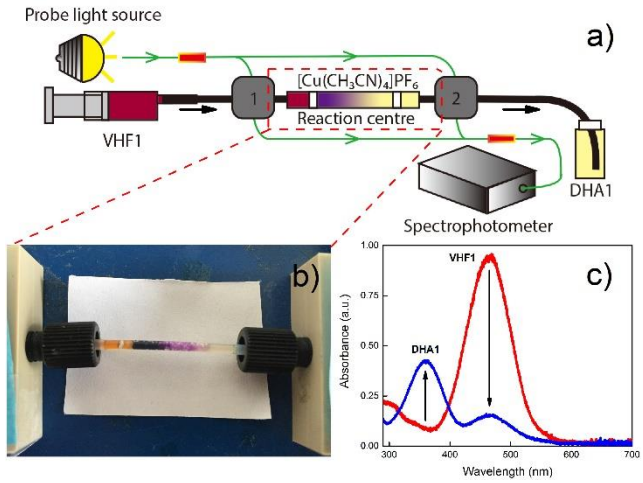

Figure 6.8. Catalytic conversion in a flow reactor. a) and b) Scheme and photo of the back-conversion setup. Boxes 1 and 2 contain flow UV-vis spectrophotometers positioned in the flow system before and after irradiation; c) UV-vis spectra before (red) and after (blue) exposure to $[Cu(CH_3CN)_4]PF_6$. *© Reproduced with permission from ChemSusChem, John Wiley and Sons.*

6.2.5 Conclusion

In this chapter, the interconversion of **DHA1/VHF1** couple was characterized in three solvents of differing polarity, where toluene was found to be the optimal solvent for further device tests. By introducing a toluene solution of **DHA1/VHF1** couple into a microfluidic chip for both indoor and outdoor demonstrations, a successful conversion was obtained with different residence times. However, it should be noted that the energy storage efficiency is still largely limited by a strong inner filter effect of the molecule. Moreover, a Cu(I) ion based salt, $[Cu(CH_3CN_4)]BF_4$, was tested as a catalytic back-conversion reactor under flow conditions. Interestingly, this copper salt works for both **AZO1** and **DHA1** systems. Yet, a more effective catalyst needs to be found to further the research into DHA derivatives applications for MOST, as the current results from the Cu(I) ion source tested are not sufficient to achieve a macroscopic heat release.

Chapter 7

MOST candidates: A brief comparison

In this thesis, three MOST candidates have been studied in detail for further application purposes, a summarized table of several key parameters can be found in table 7.1. For all three tested compounds, the absorption spectrum of the parent states is still located in the UV, and only covers a small portion of visible light. It seems that the negative photochromic materials, such as **NBD1**, are much more attractive compared to positive photochromic compounds, like **AZO1** and **DHA1**. The absorption spectrum of a photoisomer from negative photochromism can significantly decrease the usage of incoming solar light since the increasing absorption of photoisomer will waste the incoming photons in useless excitation energy losses. At the same time, it is very often that the positive photochromic photoisomer has spectral overlap with its parent state, thus forming a photostationary state. In such a situation as **DHA1**, the photoconversion process will be almost stopped due to the inner filter effect. This issue can be solved by decreasing the optical pathlength of the device while passing the solutions. However, P-type photoswitches, as the **AZO1** case, are not recommended for MOST applications, because the *cis* state of **AZO1** can be photo-back-converted to *trans* state under visible irradiation, hence in a device without an appropriate optical filter, the practical energy storage efficiency is limited. In addition, **NBD1** and **DHA1** have more promising photoisomerization quantum yields than the **AZO1** compound and are thus favored for further energy conversion purposes.

In general, single NBD unit based photoswitchable compounds have higher energy storage efficiency compare to single AZO and DHA based materials, because of the band strength

and relatively low molecular weight. In this thesis, **NBD1** (88.5 kJ mol^{-1}) has a high energy storage density compare to **AZO1** (52.0 kJ mol^{-1}) and **DHA1** (35.2 kJ mol^{-1} in theory), and is able to release an absolute temperature of 63.4 °C. Due to catalyst limitations, macroscopic heat release cannot be performed for **AZO1** and **DHA1**. The limitation for **NBD1** to release even higher energy was identified as a solubility limit. Therefore, efforts on increasing the solubility or how to make a robust neat sample are goals for the future.

Table 7.1. Key parameters summarized for three MOST candidates which have been integrated into devices in this thesis.

	λ_{onset} (nm)	λ_{max} (nm)	ε_{max} (M^{-1} cm^{-1})	Φ_{iso} (%)	$t_{1/2}$	Solubility (M)	Degradation rate	$\Delta H_{storage}$ (kJ mol^{-1})
NBD1	326	326	1.3×10^4	61%	30 days	1.52	0.14%	89
AZO1	513	350	2.5×10^4	21%	36 hours	neat	N/A over 203 cycles	52
DHA1	452	360	1.6×10^4	60%	25 hours	0.21	0.01%	35

Chapter 8

Concluding remarks and outlooks

Molecular solar thermal energy storage is a technology that stores solar energy in the form of chemical bonds, and this energy can later be released as heat using thermal or catalytic activation. This thesis focused on the characterization of different proposed MOST candidates and then these devices were evaluated for developing towards real-world applications. Three MOST candidates, including an NBD derivative (**NBD1**), an AZO derivative (**AZO1**) and a DHA derivative (**DHA1**) have been systematically studied and evaluated for application purposes. Among the three candidates, **NBD1** had better spectroscopic behavior than **AZO1** and **DHA1**, because of its intrinsic negative photochromism after conversion by light.

Since **NBD1** can be produced in large quantities, there was an attempt to modify the compound by extending the conjugation through the C2 position. As a result, the absorption spectra of the modified derivatives were red-shifted, however, the energy storage half-lives have been significantly decreased to the range of a few minutes. Alternatively, with structural modifications in the C7 position, the half-life can be largely improved, which confirms that the increasing steric bulk in the NBD form positively extends the half-life, as discovered in previous work, while, at the same time, leaves the possibility of polymerizing NBDs through functionalities introduced to the C7 position in the future.

All three photoswitches showed robust charging and discharging cycles under either light or thermal conditions. The energy storage period can be varied between days to months under room temperature of around 25 °C. Additionally, as discussed before, Jevric et al. discovered that in donor-acceptor NBDs, steric bulky substituents placed in the *ortho* position of the aromatic ring could hamper the rotation motion of the side groups along the back-

conversion path, consequently resulting in exceptionally long half-lives without significantly affecting other photophysical properties.[123, 130]

To further evaluate those compounds for real MOST applications, all three compounds focused upon in this work were integrated into solar devices. Photoswiches **DHA1** and **AZO1** were tested in a microfluidic chip on the lab-scale. In both cases, the energy storage efficiency detected was very low due to strong inner filter effects. Due to the photo back-conversion of **AZO1**-*cis* with a clear photostationary state, only **DHA1** and **NBD1** were further evaluated with the outdoor solar facility. However, similar to in the lab-scale tests, huge efficiency losses for both cases were observed. It is almost certain that the inner filter effect has been amplified by the long pathlength of the solar collection tube and could be a result of running them at high concentrations.

The catalytic back-conversion was then tested for three candidates in the device setup. Following previous literature, the pre-converted **VHF1** solution was successfully back converted to its initial state by using $[Cu(CH_3CN)_4]PF_6$. This Cu(I) salt has also been used and provides a positive effect on the **AZO1** *cis* to *trans* back conversion. To better understand the functional mechanism of the back-conversion with $[Cu(CH_3CN)_4]PF_6$, a detailed DFT calculation was performed for **AZO1**, showing that the coordination of the copper ion can decrease the isomerization barrier enough to reduce the storage half-life by 4 orders of magnitude. However, the effect of such a catalyst is still not effective enough to be applied to macroscopic heat generation.

Even in view of the high energy density of the **NBD1** compound, a fast and efficient catalyst needs to be discovered. After screening 14 different metal complexes as well as salts, the most efficient catalyst found for **QC1** was Cobalt phthalocyanine. To fix the catalyst on a support, CoPc was physisorbed onto activated carbon. In order to practically demonstrate the functionality of fixed bed CoPc@C, a vacuum-based heat release device was constructed. With a saturated, pre-converted **QC1** solution, an absolute temperature of 63.4 °C was successfully achieved, which matched well with the theoretical prediction. For a further understanding of the catalytic functionality, a detailed DFT calculation was performed. The results implied a low energy barrier in agreement with the observed experimental data.

Future research directions need to focus on these existing challenges. Specifically, liquid MOST or highly concentrated MOST solution needs to be further investigated.[180] Additionally, a negative photochromism with a parent state that is redshifted, or a positive photochromism with a photoisomer that is blue-shifted needs to be synthesized because a slight spectrum overlap between parent state and photoisomer will be significantly amplified by the inner filter effect in large scale devices. In addition, a strategy of extending the storage half-lives while also increasing energy storage density needs to be further investigated, potentially by introducing bulky substituents on C7 position of **NBD1** and extending the π-conjugation at the same time. Concerning the photoisomerization quantum yield, it is still unclear how to chemically design desired values, and this needs more attention in the future. As mentioned before, from a previous theoretical study, it was predicted that the maximum solar energy conversion efficiency is at least 10.6% at a 1.89 eV S_1-S_0 gap (corresponding to 656 nm), thus there remains a huge space (theoretical maximum energy storage efficiency with different optical pathlength in this thesis for **NBD1**: 0.51%, **AZO1**: 0.88% and **DHA1**:0.81%) for the development of current MOST systems in the future.[147] Additionally, for energy collection after storage, it is necessary to develop a universal catalyst that can work efficiently for each MOST candidate, while remaining stable on a fixed support. The author suggests testing metal-organic framework based catalysts, functionalized resins, and nanoparticles for such requirements in the future.

In order to speed up the evaluation process while obtaining a new molecule, it is worthwhile to establish a characterization protocol for future MOST candidate tests. Therefore, the following points are suggested as a checklist to criticize the functionality of a certain MOST candidate in the future. It is necessary to measure:

1. Absorption spectrum for both parent molecule and photoisomer molecule
2. Photoisomerization quantum yield
3. Energy storage half-life
4. Cyclability
5. Energy storage density
6. Theoretical maximum energy storage efficiency
7. Experimental energy storage efficiency evolution over residence time in an irradiated device

8. Theoretical maximum heat release temperature
9. Maximum experimental heat release temperature
10. Catalyst reaction constant
11. Catalyst TON, TOF number
12. Solvent effect of the MOST candidate

Together with a more advanced flow system, new devices to continue testing full cycles of the MOST candidates can be addressed by applying such established evaluation protocols, hence efficiently testing potential MOST systems. To further realize a lab-to-site technology transfer, it is also necessary to consider material hazards and estimate material costs for future industrialization. With all the above research directions in mind, the author of this thesis believes that MOST has great potential to be an optimal green energy resource in the near future.

References

1. *BP Statistical Review of World Energy*, BP plc, 2019.

2. United Nations, *World Population Prospects 2019: Highlights*, 2019.

3. N. S. Lewis and D. G. Nocera, *Proceedings of the National Academy of Sciences*, 2006, **103**, 15729-15735.

4. *World energy balances: Overview*, IEA International Energy Agency, 2019.

5. *CO_2 emissions from fuel combustion: Highlights*, IEA International Energy Agency, 2018.

6. *Energy and climate change*, IEA International Energy Agency, 2015.

7. R. S. Lindzen, *Bulletin of the American Meteorological Society*, 1990, **71**, 288-299.

8. D. B. Botkin, H. Saxe, M. B. Araújo, R. Betts, R. H. W. Bradshaw, T. Cedhagen, P. Chesson, T. P. Dawson, J. R. Etterson, D. P. Faith, S. Ferrier, A. Guisan, A. S. Hansen, D. W. Hilbert, C. Loehle, C. Margules, M. New, M. J. Sobel and D. R. B. Stockwell, *BioScience*, 2007, **57**, 227-236.

9. M. P. McCarthy, M. J. Best and R. A. Betts, *Geophysical Research Letters*, 2010, **37**.

10. E. S. Zavaleta, B. D. Thomas, N. R. Chiariello, G. P. Asner, M. R. Shaw and C. B. Field, *Proceedings of the National Academy of Sciences*, 2003, **100**, 9892-9893.

11. N. W. Arnell and N. S. Reynard, *Journal of Hydrology*, 1996, **183**, 397-424.

12. R. L. Peters, *Forest Ecology and Management*, 1990, **35**, 13-33.

13. J. Joireman, H. Barnes Truelove and B. Duell, *Journal of Environmental Psychology*, 2010, **30**, 358-367.

14. K. Emanuel, *Weather, Climate, and Society*, 2011, **3**, 261-268.

15. L. G. Sorenson, R. Goldberg, T. L. Root and M. G. Anderson, *Climatic Change*, 1998, **40**, 343-369.

16. *Adoption of the Paris agreement*, UN FCCC conference of the Parties (COP), 2015.

17. *Renewables information: Overview*, IEA International Energy Agency, 2019.

18. R. Perez and M. Perez, *IEA-SHCP-Newsletter*, 2009, **50**.

19. R. Perez and M. Perez, *IEA-SHCP-Newsletter*, 2015, **62**.

20. K. Mertens, *Photovoltaics: Fundamentals, Technology, and Practice*, Wiley, 2018.

21. L. Chaar, L. Lamont and N. Zein, *Renewable and Sustainable Energy Reviews*, 2011, **15**, 2165-2175.

22. A. F. Collings and C. Critchley, *Artificial Photosynthesis: From Basic Biology to Industrial Application*, Wiley, 2005.

23. T. J. Meyer, *Accounts of Chemical Research*, 1989, **22**, 163-170.

24. D. Gust, T. A. Moore and A. L. Moore, *Accounts of Chemical Research*, 2009, **42**, 1890-1898.

25. S. M. Hasnain, S. H. Alawaji and U. A. Elani, *Renewable Energy*, 1998, **14**, 387-392.

26. G. A. Lane, *Solar heat storage: Latent heat materials*, CRC Press,Boco Raton, FL, United States, 1983.

27. *Energy consumption in households* Eurostate Statistics Explained, 2017.

28. Z.-i. Yoshida, *Journal of Photochemistry*, 1985, **29**, 27-40.

29. K. Moth-Poulsen, D. Ćoso, K. Börjesson, N. Vinokurov, S. K. Meier, A. Majumdar, K. P. C. Vollhardt and R. A. Segalman, *Energy & Environmental Science*, 2012, **5**, 8534-8537.

30. A. Lennartson and K. Moth-Poulsen, in *Molecular Devices for Solar Energy Conversion and Storage*, eds. H. Tian, G. Boschloo and A. Hagfeldt, Springer Singapore, Singapore, 2018, DOI: 10.1007/978-981-10-5924-7_9, pp. 327-352.

31. L. Dong, Y. Feng, L. Wang and W. Feng, *Chemical Society Reviews*, 2018, **47**, 7339-7368.

32. *Solar Thermal Fuel Market*, Transparency Market Research, 2019.

33. T. Von Grotthuss, *Annalen der Physik*, 1819, **61**, 50-74.

34. H. Trommsdorff, *Annalen der Pharmacie*, 1834, **11**, 190-207.

35. D. B. Medved, *American Mineralogist*, 1954, **39**, 615-629.

36. K. P. Thakur and J. D. Pandey, *Journal of Inorganic and Nuclear Chemistry*, 1975, **37**, 645-649.

37. A. Kafizas, C. W. Dunnill and I. P. Parkin, *Physical Chemistry Chemical Physics*, 2011, **13**, 13827-13838.

38. G. Xu, G.-C. Guo, M.-S. Wang, Z.-J. Zhang, W.-T. Chen and J.-S. Huang, *Angewandte Chemie International Edition*, 2007, **46**, 3249-3251.

39. T. He and J. Yao, *Journal of Materials Chemistry*, 2007, **17**, 4547-4557.

40. T. He and J. Yao, *Journal of Photochemistry and Photobiology C: Photochemistry Reviews*, 2003, **4**, 125-143.

41. R. J. Araujo, *Contemporary Physics*, 1980, **21**, 77-84.

42. S. D. Cohen and G. A. Newman, *The Journal of Photographic Science*, 1967, **15**, 290-298.

43. G. Xu, G.-C. Guo, J.-S. Guo, S.-P. Guo, X.-M. Jiang, C. Yang, M.-S. Wang and Z.-J. Zhang, *Dalton Transactions*, 2010, **39**, 8688-8692.

44. J. Fritzsche, *Journal für Praktische Chemie*, 1866, **97**, 290-303.

45. F. Weigert, *Ber. Dtsch. Chem. Ges.*, 1909, **42**, 850-862.

46. F. Weigert, *Eder's Jahrb.*, 1909, 111.

47. R. Luther and F. Weigert, *Journal*, 1905, **53U**, 385.

48. F. Weigert, *Jahrbuch für Photographie, Kinematographie und Reproduktionsverfahren*, 1908.

49. J. Henzl, M. Mehlhorn and K. Morgenstern, *Nanotechnology*, 2007, **18**, 495502.

50. T. Fukaminato, T. Hirose, T. Doi, M. Hazama, K. Matsuda and M. Irie, *Journal of the American Chemical Society*, 2014, **136**, 17145-17154.

51. M. Irie, T. Fukaminato, T. Sasaki, N. Tamai and T. Kawai, *Nature*, 2002, **420**, 759-760.

52. S. Kawata and Y. Kawata, *Chemical Reviews*, 2000, **100**, 1777-1788.

53. M. Sauer, *Proceedings of the National Academy of Sciences of the United States of America*, 2005, **102**, 9433-9434.

54. C. E. Weston, R. D. Richardson, P. R. Haycock, A. J. P. White and M. J. Fuchter, *Journal of the American Chemical Society*, 2014, **136**, 11878-11881.

55. M. Irie, *Chemical Reviews*, 2000, **100**, 1685-1716.

56. L. Sun, Y. A. Diaz-Fernandez, T. A. Gschneidtner, F. Westerlund, S. Lara-Avila and K. Moth-Poulsen, *Chemical Society Reviews*, 2014, **43**, 7378-7411.

57. M. Jevric, S. L. Broman and M. B. Nielsen, *The Journal of Organic Chemistry*, 2013, **78**, 4348-4356.

58. S. L. Broman, S. Lara-Avila, C. L. Thisted, A. D. Bond, S. Kubatkin, A. Danilov and M. B. Nielsen, *Advanced Functional Materials*, 2012, **22**, 4249-4258.

59. B. E. Tebikachew, H. B. Li, A. Pirrotta, K. Börjesson, G. C. Solomon, J. Hihath and K. Moth-Poulsen, *The Journal of Physical Chemistry C*, 2017, **121**, 7094-7100.

60. Y. Wu, K. Eisele, M. Doroshenko, G. Algara-Siller, U. Kaiser, K. Koynov and T. Weil, *Small*, 2012, **8**, 3465-3475.

61. Y. Wang, C.-W. Ge, Y.-F. Zou, R. Lu, K. Zheng, T.-F. Zhang, Y.-Q. Yu and L.-B. Luo, *Advanced Optical Materials*, 2016, **4**, 291-296.

62. S. Scarmagnani, Z. Walsh, C. Slater, N. Alhashimy, B. Paull, M. Macka and D. Diamond, *Journal of Materials Chemistry*, 2008, **18**, 5063-5071.

63. S. Nau, C. Wolf, S. Sax and E. J. W. List-Kratochvil, *Advanced Materials*, 2015, **27**, 1048-1052.

64. A. Balamurugan and H.-i. Lee, *Macromolecules*, 2016, **49**, 2568-2574.

65. J. Li, H. K. Bisoyi, S. Lin, J. Guo and Q. Li, *Angewandte Chemie International Edition*, 2019, **58**, 16052-16056.

66. H. Wang, H. K. Bisoyi, M. E. McConney, A. M. Urbas, T. J. Bunning and Q. Li, *Advanced Materials*, 2019, **31**, 1902958.

67. H. Wang, H. K. Bisoyi, A. M. Urbas, T. J. Bunning and Q. Li, *Journal of the American Chemical Society*, 2019, **141**, 8078-8082.

68. Z.-g. Zheng, Y. Li, H. K. Bisoyi, L. Wang, T. J. Bunning and Q. Li, *Nature*, 2016, **531**, 352-356.

69. D. Kim, K. Jeong, J. E. Kwon, H. Park, S. Lee, S. Kim and S. Y. Park, *Nature Communications*, 2019, **10**, 3089.

70. J. B. Birks, J. H. Appleyard and R. Pope, *Photochemistry and Photobiology*, 1963, **2**, 493-495.

71. H. Bouas-Laurent, A. Castellan and J.-P. Desvergne, *Journal*, 1980, **52**, 2633.

72. M. Daney, C. Vanucci, J. P. Desvergne, A. Casterllan and H. Bouas-Laurent, *Tetrahedron Letters*, 1985, **26**, 1508.

73. T. Tamaki, T. Kokubu and K. Ichimura, *Tetrahedron*, 1987, **43**, 1485-1494.

74. A. Dawn, N. Fujita, S. Haraguchi, K. Sada and S. Shinkai, *Chemical Communications*, 2009, DOI: 10.1039/B820565E, 2100-2102.

75. J.-F. Xu, Y.-Z. Chen, L.-Z. Wu, C.-H. Tung and Q.-Z. Yang, *Organic Letters*, 2013, **15**, 6148-6151.

76. P. G. Frank, B. T. Tuten, A. Prasher, D. Chao and E. B. Berda, *Macromolecular Rapid Communications*, 2014, **35**, 249-253.

77. J. Splitter and M. Calvin, *The Journal of Organic Chemistry*, 1958, **23**, 651-651.

78. J. Hamer and A. Macaluso, *Chemical Reviews*, 1964, **64**, 473-495.

79. M. Strmiskova, D. A. Bilodeau, M. Chigrinova and J. P. Pezacki, *Canadian Journal of Chemistry*, 2018, **97**, 1-6.

80. H. Giezendanner, H. J. Rosenkranz, H.-J. Hansen and H. Schmid, *Helvetica Chimica Acta*, 1973, **56**, 2588-2611.

81. G. Jones and B. R. Ramachandran, *The Journal of Organic Chemistry*, 1976, **41**, 798-801.

82. G. Jones and L. J. Turbini, *The Journal of Organic Chemistry*, 1976, **41**, 2362-2367.

83. I. Ioffe and A. Granovsky, *Journal of Chemical Theory and Computation*, 2013, **9**, 4973–4990.

84. D. H. Waldeck, *Chemical Reviews*, 1991, **91**, 415-436.

85. S. Aloïse, R. Yibin, I. Hamdi, G. Buntinx, A. Perrier, F. Maurel, D. Jacquemin and M. Takeshita, *Physical Chemistry Chemical Physics*, 2014, **16**, 26762-26768.

86. S. Fukumoto, T. Nakashima and T. Kawai, *European Journal of Organic Chemistry*, 2011, **2011**, 5047-5053.

87. S. Fukumoto, T. Nakashima and T. Kawai, *Angewandte Chemie International Edition*, 2011, **50**, 1565-1568.

88. W. Li, C. Jiao, X. Li, Y. Xie, K. Nakatani, H. Tian and W. Zhu, *Angewandte Chemie*, 2014, **126**, 4691-4695.

89. Y. Ishibashi, M. Mukaida, M. Falkenström, H. Miyasaka, S. Kobatake and M. Irie, *Physical Chemistry Chemical Physics*, 2009, **11**, 2640-2648.

90. C.-L. Sun, C. Wang and R. Boulatov, *ChemPhotoChem*, 2019, **3**, 268-283.

91. A. M. Kolpak and J. C. Grossman, *Nano Letters*, 2011, **11**, 3156-3162.

92. Z. Wang, R. Losantos, D. Sampedro, M.-a. Morikawa, K. Börjesson, N. Kimizuka and K. Moth-Poulsen, *Journal of Materials Chemistry A*, 2019, **7**, 15042-15047.

93. A. Lennartson, A. Roffey and K. Moth-Poulsen, *Tetrahedron Letters*, 2015, **56**, 1457-1465.

94. H. Taoda, K. Hayakawa, K. Kawase and H. Yamakita, *Journal of Chemical Engineering of Japan*, 1987, **20**, 265-270.

95. K. Ishiba, M.-a. Morikawa, C. Chikara, T. Yamada, K. Iwase, M. Kawakita and N. Kimizuka, *Angewandte Chemie International Edition*, 2015, **54**, 1532-1536.

96. T. J. Kucharski, N. Ferralis, A. M. Kolpak, J. O. Zheng, D. G. Nocera and J. C. Grossman, *Nature Chemistry*, 2014, **6**, 441.

97. M. Zhu and H. Zhou, *Organic & Biomolecular Chemistry*, 2018, **16**, 8434-8445.

98. A. A. Beharry, L. Wong, V. Tropepe and G. A. Woolley, *Angewandte Chemie International Edition*, 2011, **50**, 1325-1327.

99. X. Liang, T. Mochizuki and H. Asanuma, *Small*, 2009, **5**, 1761-1768.

100. O. Sadovski, A. A. Beharry, F. Zhang and G. A. Woolley, *Angewandte Chemie International Edition*, 2009, **48**, 1484-1486.

101. T. Goldau, K. Murayama, C. Brieke, S. Steinwand, P. Mondal, M. Biswas, I. Burghardt, J. Wachtveitl, H. Asanuma and A. Heckel, *Chemistry – A European Journal*, 2015, **21**, 2845-2854.

102. K. Masutani, M.-a. Morikawa and N. Kimizuka, *Chemical Communications*, 2014, **50**, 15803-15806.

103. A. Kunz, A. H. Heindl, A. Dreos, Z. Wang, K. Moth-Poulsen, J. Becker and H. A. Wegner, *ChemPlusChem*, 2019, **84**, 1145-1148.

104. J. Olmsted, J. Lawrence and G. G. Yee, *Solar Energy*, 1983, **30**, 271-274.

105. K. Edel, X. Yang, J. S. A. Ishibashi, A. N. Lamm, C. Maichle-Mössmer, Z. X. Giustra, S.-Y. Liu and H. F. Bettinger, *Angewandte Chemie International Edition*, 2018, **57**, 5296-5300.

106. C. Brieke and A. Heckel, *Chemistry – A European Journal*, 2013, **19**, 15726-15734.

107. M. Hammarson, J. R. Nilsson, S. Li, P. Lincoln and J. Andréasson, *Chemistry – A European Journal*, 2014, **20**, 15855-15862.

108. H. Zulfikri, M. A. J. Koenis, M. M. Lerch, M. Di Donato, W. Szymański, C. Filippi, B. L. Feringa and W. J. Buma, *Journal of the American Chemical Society*, 2019, **141**, 7376-7384.

109. R. Saha, A. Devaraj, S. Bhattacharyya, S. Das, E. Zangrando and P. S. Mukherjee, *Journal of the American Chemical Society*, 2019, **141**, 8638-8645.

110. N. Mallo, P. Brown, H. Iranmanesh, T. Macdonald, M. Teusner, J. Harper, G. Ball and J. Beves, *Chem. Commun.*, 2016, **52**.

111. V. A. Bren, A. D. Dubonosov, V. I. Minkin and V. A. Chernoivanov, *Russian Chemical Reviews*, 1991, **60**, 451-469.

112. A. Dubonosov, V. Bren' and V. Minkin, 2003, pp. 17-11.

113. M. Quant, A. Lennartson, A. Dreos, M. Kuisma, P. Erhart, K. Börjesson and K. Moth-Poulsen, *Chemistry – A European Journal*, 2016, **22**, 13265-13274.

114. M. J. Kuisma, A. M. Lundin, K. Moth-Poulsen, P. Hyldgaard and P. Erhart, *The Journal of Physical Chemistry C*, 2016, **120**, 3635-3645.

115. A. Dreos, K. Börjesson, Z. Wang, A. Roffey, Z. Norwood, D. Kushnir and K. Moth-Poulsen, *Energy & Environmental Science*, 2017, **10**, 728-734.

116. K. Jorner, A. Dreos, R. Emanuelsson, O. El Bakouri, I. Fdez. Galván, K. Börjesson, F. Feixas, R. Lindh, B. Zietz, K. Moth-Poulsen and H. Ottosson, *Journal of Materials Chemistry A*, 2017, **5**, 12369-12378.

117. B. E. Tebikachew, F. Edhborg, N. Kann, B. Albinsson and K. Moth-Poulsen, *Physical Chemistry Chemical Physics*, 2018, **20**, 23195-23201.

118. Z. Wang, A. Roffey, R. Losantos, A. Lennartson, M. Jevric, A. U. Petersen, M. Quant, A. Dreos, X. Wen, D. Sampedro, K. Börjesson and K. Moth-Poulsen, *Energy & Environmental Science*, 2019, **12**, 187-193.

119. M. D. Kilde, M. Mansø, N. Ree, A. U. Petersen, K. Moth-Poulsen, K. V. Mikkelsen and M. B. Nielsen, *Organic & Biomolecular Chemistry*, 2019, **17**, 7735-7746.

120. A. U. Petersen, A. I. Hofmann, M. Fillols, M. Mansø, M. Jevric, Z. Wang, C. J. Sumby, C. Müller and K. Moth-Poulsen, *Advanced Science*, 2019, **6**, 1900367.

121. C. Schuschke, C. Hohner, M. Jevric, A. Ugleholdt Petersen, Z. Wang, M. Schwarz, M. Kettner, F. Waidhas, L. Fromm, C. J. Sumby, A. Görling, O. Brummel, K. Moth-Poulsen and J. Libuda, *Nature Communications*, 2019, **10**, 2384.

122. M. Quant, A. Hamrin, A. Lennartson, P. Erhart and K. Moth-Poulsen, *The Journal of Physical Chemistry C*, 2019, **123**, 7081-7087.

123. M. Jevric, Z. Wang, A. U. Petersen, M. Mansø, C. J. Sumby, M. B. Nielsen and K. Moth-Poulsen, *European Journal of Organic Chemistry*, 2019, **2019**, 2354-2361.

124. M. Mansø, B. E. Tebikachew, K. Moth-Poulsen and M. B. Nielsen, *Organic & Biomolecular Chemistry*, 2018, **16**, 5585-5590.

125. M. Mansø, M. D. Kilde, S. K. Singh, P. Erhart, K. Moth-Poulsen and M. B. Nielsen, *Physical Chemistry Chemical Physics*, 2019, **21**, 3092-3097.

126. M. Mansø, A. U. Petersen, Z. Wang, P. Erhart, M. B. Nielsen and K. Moth-Poulsen, *Nature Communications*, 2018, **9**, 1945.

127. A. U. Petersen, M. Jevric and K. Moth-Poulsen, *European Journal of Organic Chemistry*, 2018, **2018**, 4465-4474.

128. M. Kuisma, A. Lundin, K. Moth-Poulsen, P. Hyldgaard and P. Erhart, *ChemSusChem*, 2016, **9**, 1786-1794.

129. V. Gray, A. Lennartson, P. Ratanalert, K. Börjesson and K. Moth-Poulsen, *Chemical Communications*, 2014, **50**, 5330-5332.

130. M. Jevric, A. U. Petersen, M. Mansø, S. Kumar Singh, Z. Wang, A. Dreos, C. Sumby, M. B. Nielsen, K. Börjesson, P. Erhart and K. Moth-Poulsen, *Chemistry – A European Journal*, 2018, **24**, 12767-12772.

131. F. Waidhas, M. Jevric, L. Fromm, M. Bertram, A. Görling, K. Moth-Poulsen, O. Brummel and J. Libuda, *Nano Energy*, 2019, **63**, 103872.

132. H. Goerner, C. Fischer, S. Gierisch and J. Daub, *The Journal of Physical Chemistry*, 1993, **97**, 4110-4117.

133. J. Daub, T. Knöchel and A. Mannschreck, *Angewandte Chemie*, 1984, **96**, 980-981.

134. H. Spreitzer and J. Daub, *Chemistry – A European Journal*, 1996, **2**, 1150-1158.

135. J. Ern, M. Petermann, T. Mrozek, J. Daub, K. Kuldová and C. Kryschi, *Chemical Physics*, 2000, **259**, 331-337.

136. S. L. Broman, M. Å. Petersen, C. G. Tortzen, A. Kadziola, K. Kilså and M. B. Nielsen, *Journal of the American Chemical Society*, 2010, **132**, 9165-9174.

137. V. De Waele, U. Schmidhammer, T. Mrozek, J. Daub and E. Riedle, *Journal of the American Chemical Society*, 2002, **124**, 2438-2439.

138. S. Broman, S. Brand, C. Parker, M. Petersen, C. Tortzen, A. Kadziola, K. Kilså and M. Nielsen, *Arkivoc*, 2011, **2011**, 51-67.

139. T. Mrozek, H. Görner and J. Daub, *Chemistry – A European Journal*, 2001, **7**, 1028-1040.

140. S. L. Broman and M. B. Nielsen, *Physical Chemistry Chemical Physics*, 2014, **16**, 21172-21182.

141. L. Gobbi, P. Seiler, F. Diederich, V. Gramlich, C. Boudon, J.-P. Gisselbrecht and M. Gross, *Helvetica Chimica Acta*, 2001, **84**, 743-777.

142. M. Cacciarini, A. B. Skov, M. Jevric, A. S. Hansen, J. Elm, H. G. Kjaergaard, K. V. Mikkelsen and M. Brøndsted Nielsen, *Chemistry – A European Journal*, 2015, **21**, 7454-7461.

143. J. Mogensen, O. Christensen, M. D. Kilde, M. Abildgaard, L. Metz, A. Kadziola, M. Jevric, K. V. Mikkelsen and M. B. Nielsen, *European Journal of Organic Chemistry*, 2019, **2019**, 1986-1993.

144. R. Boese, J. K. Cammack, A. J. Matzger, K. Pflug, W. B. Tolman, K. P. C. Vollhardt and T. W. Weidman, *Journal of the American Chemical Society*, 1997, **119**, 6757-6773.

145. Y. Kanai, V. Srinivasan, S. K. Meier, K. P. C. Vollhardt and J. C. Grossman, *Angewandte Chemie International Edition*, 2010, **49**, 8926-8929.

146. M. R. Harpham, S. C. Nguyen, Z. Hou, J. C. Grossman, C. B. Harris, M. W. Mara, A. B. Stickrath, Y. Kanai, A. M. Kolpak, D. Lee, D.-J. Liu, J. P. Lomont, K. Moth-Poulsen, N. Vinokurov, L. X. Chen and K. P. C. Vollhardt, *Angewandte Chemie International Edition*, 2012, **51**, 7692-7696.

147. K. Börjesson, A. Lennartson and K. Moth-Poulsen, *ACS Sustainable Chemistry & Engineering*, 2013, **1**, 585-590.

148. K. Börjesson, A. Lennartson and K. Moth-Poulsen, *Journal of Fluorine Chemistry*, 2014, **161**, 24-28.

149. V. A. Barachevsky, *Review Journal of Chemistry*, 2017, **7**, 334-371.

150. C. Zhang, Z. Zhang, M. Fan and W. Yan, *Dyes and Pigments - DYE PIGMENT*, 2008, **76**, 832-835.

151. A. Dubonosov, V. Bren' and V. Chernoivanov, *Russian Chemical Reviews*, 2007, **71**, 917.

152. J. D. J. Ingle and S. R. Crouch, *New Jersey: Prentice Hall*, 1988.

153. K. Stranius and K. Börjesson, *Scientific Reports*, 2017, **7**, 41145.

154. C. G. Hatchard and C. A. Parker, *Proceedings of the Royal Society of London. Series A, Mathematical and Physical Sciences*, 1956, **235**, 518-536.

155. J. Boutagy and R. Thomas, *Chemical Reviews*, 1974, **74**, 87-99.

156. G. Wittig and U. Schöllkopf, *Chemische Berichte*, 1954, **87**, 1318-1330.

157. O. Diels and K. Alder, in *Justus Liebig's Annalen der Chemie* 1931, vol. 490, ch. XI. Diene synthesis of cyclopentadiene, cyclohexadiene and butadiene with acetylenedicarboxylic acid and its esters, 236-242.

158. Hyman I, *Bicycloheptadienes*, Application: BE Patent BE 498176, 1951.

159. S. J. Cristol and R. L. Snell, *Journal of the American Chemical Society*, 1958, **80**, 1950-1952.

160. W. Dauben, *Tetrahedron*, 1961, **15**, 197-201.

161. G. S. Hammond, N. J. Turro and A. Fischer, *Journal of the American Chemical Society*, 1961, **83**, 4674-4675.

162. R. B. Woodward and R. Hoffmann, *Angewandte Chemie International Edition in English*, 1969, **8**, 781-853.

163. R. B. Woodward and R. Hoffmann, *Journal of the American Chemical Society*, 1965, **87**, 395-397.

164. C. Qin, Z. Zhao and S. R. Davis, *Journal of Molecular Structure: THEOCHEM*, 2005, **728**, 67-70.

165. P. R. Khoury, J. D. Goddard and W. Tam, *Tetrahedron*, 2004, **60**, 8103-8112.

166. D. S. Kabakoff, J. C. G. Buenzli, J. F. M. Oth, W. B. Hammond and J. A. Berson, *Journal of the American Chemical Society*, 1975, **97**, 1510-1512.

167. R. Löw, T. Rusch, T. Moje, F. Röhricht, O. Magnussen and R. Herges, *Beilstein Journal of Organic Chemistry*, 2019, **15**, 1815-1821.

168. Y. Mekonnen, A. Sundararajan and A. Sarwat, *A review of cathode and anode materials for lithium-ion batteries*, 2016.

169. T. E. Shubina and T. Clark, *Zeitschrift fur Naturforschung - Section B Journal of Chemical Sciences*, 2010, **65**, 347-356.

170. J. Handzlik, M. Stosur, A. Kochel and T. Szymańska-Buzar, *Inorganica Chimica Acta*, 2008, **361**, 502-512.

171. F. Ghani, J. Kristen and H. Riegler, *Journal of Chemical & Engineering Data*, 2012, **57**, 439-449.

172. H. Shirakawa, *Angewandte Chemie International Edition*, 2001, **40**, 2574-2580.

173. A. Goulet-Hanssens, M. Utecht, D. Mutruc, E. Titov, J. Schwarz, L. Grubert, D. Bléger, P. Saalfrank and S. Hecht, *Journal of the American Chemical Society*, 2017, **139**, 335-341.

174. E. Titov, L. Lysyakova, N. Lomadze, A. V. Kabashin, P. Saalfrank and S. Santer, *The Journal of Physical Chemistry C*, 2015, **119**, 17369-17377.

175. A. M. Sanchez, M. Barra and R. H. de Rossi, *The Journal of Organic Chemistry*, 1999, **64**, 1604-1609.

176. S. Ciccone and J. Halpern, *Canadian Journal of Chemistry*, 1959, **37**, 1903-1910.

177. Z. Wang, J. Udmark, K. Börjesson, R. Rodrigues, A. Roffey, M. Abrahamsson, M. B. Nielsen and K. Moth-Poulsen, *ChemSusChem*, 2017, **10**, 3049-3055.

178. J. Daub, S. Gierisch, T. Knöchel and E. Salbeck, *Journal*, 1986, **41**, 1151.

179. *Solvents and Solvent Effects in Organic Chemistry*, Wiley-VCH Publishers, 3rd ed. edn., 2003.

180. A. Dreos, Z. Wang, J. Udmark, A. Ström, P. Erhart, K. Börjesson, M. B. Nielsen and K. Moth-Poulsen, *Advanced Energy Materials*, 2018, **8**, 1703401.